PROJECT COMPLETION REPORT FOR RPS PROJECTS

(Please include sufficient details in sections 8-10 so as to facilitate proper evaluation of your project.)

File No.: 8-15/RIFD/RPS/POLICY-1/2016-17 dated 02/08/2017
(as mentioned in sanction letter)

Date of Sanction: 02/08/2017

Subject Area: Medical Image Processing

1. Principal Investigator: Prof. Bhabesh Deka
   (Name & address) Department of Electronics and Communication Engineering
   Tezpur University, Napaam, Tezpur, Assam, India, PIN: 784028

2. Project Title: Development of Parallel Processing Embedded Hardware for Super-resolution of Diffusion weighted and Spectroscopic Magnetic Resonance Images

3. Total Cost of the Project: 16, 47,059/-

4. Date of Commencement of the Project: October, 2017

5. Duration of the Project: 3 Years

6. Date of Completion: 31/12/2020

7. Objectives of the Project:

   I. To design a single image SR (SISR) algorithm using the concept of parallel computing

   II. To implement SISR techniques using the GP-GPU hardware

   III. To design and develop novel approaches for creating GP-GPU modules of single image super-resolution reconstruction

   IV. To focus on real-time operability and optimal resource utilizations

   V. To evaluate and compare performances of different algorithms for setting benchmarks for super-resolution reconstruction of DW and Spectroscopic MR images

8. Salient Research Achievements:

   Please find details in Annexure 1

   8.1 New Findings/Achievements/IPR Potential:

   - Single image super-resolution based on sparse representations over a learned overcomplete dictionary for DW and MRS images.
   - Single image super-resolution based on sparse representations based coupled overcomplete dictionaries are learnt using DW and MRS images and utilized them to extract a priori HR information.

- MR image super-resolution reconstruction using sparse representation on patch-wise of high-resolution patches from low-resolution feature patches pairs.

- MR image super-resolution reconstruction not only exploits the sparsity of MR image but also utilize the non-local self-similarity of patches of the input LR image as prior knowledge.

- Hardware implemented using the GP-GPU based parallel along with sequential for real clinical applications of MR images.

8.2 Product/Process Developed: A novel singe image super-resolution technique is developed for Diffusion weighted and Spectroscopic Magnetic Resonance Images.

8.3 Patent(s) Applied for/Taken, if any: NA

8.4 B. Tech. Project / M. Tech Thesis /: YES

B.Tech. Project: 4 Nos.
M.Tech Thesis: 2 Nos.
Ph.D., if any
Consultancy

9. Conclusions Summarizing the Achievements Indicating the Scope for Future Work.
We demonstrate a novel SISR method using sparse reconstruction based on image sparsity using trained dictionary and non-local self-similarity and that the SISR algorithm based on the sparsity over learned overcomplete dictionary along with a non-local TV regularization provides consistent SR outputs for clinical DW and MRS images at different upscale ratios. Extraction of prior information both external and internal is proved to be very efficient in preserving detailed information in super-resolved clinical DW and MRS images. Visual and quantitative comparisons with state-of-the-art SR methods have demonstrated the superiority of the proposed method. It is validated both for real MR and synthetic images; found its potential to preserve fine details and structures at different upscaling ratios. Finally, use of Multicore parallel pro cessing or general-purpose graphics processing units (GP-GPUs) hardware to get computationally efficient results, makes the proposed algorithm not only highly effective, but also practically doable. Moreover, at present, the model we use assumes that the available LR image is noise free, which would not be the case every time. For noisy image, image denoising is required prior to super resolution algorithm.

10. List of Publications Arising from the Project (please give Author (s), Title, Journal and Year):

1. Bhabesh Deka, Sumit Datta, Helal Uddin Mullah, and Suman Hazarika, "Diffusion-weighted and spectroscopic MRI super-resolution using sparse representations," Biomedical Signal Processing and Control, vol. 60, 2020.
2. Bhabesh Deka, Helal Uddin Mullah, Sumit Datta, Vijaya Lakshmi, and Rajarajeswari Ganesan, "Sparse Representation based Super-Resolution of MRI Images with Non-Local Total Variation Regularization," SN Computer Science, Springer, 2020.
3. Bhabesh Deka, Helal Uddin Mullah, Sumit Datta, Vijaya Lakshmi, and Rajarajeswari Ganesan, "Sparse Representation Based Super-Resolution of MRI Images with Non-Local Total Variation Regularization," in International Conference on Pattern Recognition and Machine Intelligence, pp. 78-86. Springer, 2019.

Dated: 11/02/2021

Principal Investigator

Registrar/Director/Principal
(Signature & Seal)
Registrar
Tezpur University

(Investigators may please note that sections 8-10 of the report will serve as essential inputs for experts to judge the success of the project. These must therefore be included in sufficient detail.)

FORMAT
For
UTILIZATION CERTIFICATE
(FY 2017-18)

Sanction Letter No. 8-15/RIFD/RPS/POLICY-1/2016-17, **Date:** 2 August 2017

A. NON-RECURRING

Sl. No.	Name of the Equipment Procured	Amount Sanctioned (₹)	Amount Released (₹)	Amount Utilized (₹)	Unspent Balance (₹)
	Not applicable	₹ 14,00,000.00	₹ 14,00,000.00	NIL	14,00,000.00

B. RECURRING

Sl. No.	Name of the Expenses	Sanctioned Amount (₹)	Amount released for FY 2017-18 (₹)	Amount Utilized (₹)	Unspent Balance (₹)
	Not applicable	2,47,059.00	2,22,353.00	NIL	2,22,353.00

Certified that the grant has been utilized for the purpose for which it was sanctioned in accordance with the "Terms and Conditions" attached to the grant. If, as a result of check or audit objection some irregularity is noticed at a later stage, action will be taken to refund, adjust or regularize the amount objected to.

18/9/18

Finance Officer
& Seal)
Finance Officer
Tezpur University
Dated:

Registrar /Principal/ Director (Signature
(Signature & Seal)
Registrar
Tezpur University
Tezpur University
Napaam, Tezput, Assam-784028

Note: The Utilization Certificate (UC) will be signed by the Registrar/ Finance Officer in the case of Universities, Principals in the case of Colleges and Executive Heads of other Institutions. The Provisional UC may be countersigned by the internal auditors wherever the system of the internal audit exists. In case of the Self Financing/ Private Institutions, UC has to be signed by a Chartered Accountant.

* This is to be submitted every financial year.

FORMAT
For
UTILIZATION CERTIFICATE
(1 April 2018 - 15th August, 2018)

Sanction Letter No. 8-15/RIFD/RPS/POLICY-1/2016-17, **Date:** 2 August 2017

A. NON-RECURRING

Sl. No.	Name of the Equipment Procured	Amount Sanctioned (₹)	Amount released (₹)	Amount Utilized (₹)	Unspent Balance (₹)
1	Workstations with GP-GPU Hardware	14,00,000.00	14,00,000.00	8,47,770.00	5,52,230.00

B. RECURRING

<table>
<tr><th>Sl. No.</th><th>Name of the Expenses</th><th>Amount Sanctioned (₹)</th><th>Amount released for FY 2017-18 (₹)</th><th>Amount Utilized (₹)</th><th>Unspent Balance (₹)</th></tr>
<tr><td>1</td><td>Traveling</td><td rowspan="2">2,47,059.00</td><td rowspan="2">2,22,353.00</td><td>6,056.00</td><td rowspan="3">2,04,840.00</td></tr>
<tr><td>2</td><td>Consumables / Stationeries</td><td>11,457.00</td></tr>
<tr><td colspan="2">Total</td><td>2,47,059.00</td><td>2,22,353.00</td><td>17,513.00</td></tr>
</table>

Certified that the grant has been utilized for the purpose for which it was sanctioned in accordance with the "Terms and Conditions" attached to the grant. If, as a result of check or audit objection some irregularity is noticed at a later stage, action will be taken to refund, adjust or regularize the amount objected to.

18/9/18

Finance Officer & Seal)
Finance Officer
Tezpur University
Dated:

Registrar/Principal/ Director (Signature (Signature & Seal)
Registrar
Tezpur University
Tezpur University
Napaam, Tezput, Assam-784028

Note: The Utilization Certificate (UC) will be signed by the Registrar/ Finance Officer in the case of Universities, Principals in the case of Colleges and Executive Heads of other Institutions. The Provisional UC may be countersigned by the internal auditors wherever the system of the internal audit exists. In case of the Self Financing/ Private Institutions, UC has to be signed by a Chartered Accountant.

* This is to be submitted every financial year.

Research Promotion Scheme

FORMAT FOR STATEMENT OF EXPENDITURE

(1st April 2018 - 15th August 2018)

AICTE File No. : 8-15/RIFD/RPS/POLICY-1/2016-17, **Date:** 2 August 2017

Title of the RPS Project : Development of Parallel Processing Embedded Hardware for Super-Resolution of Diffusion Weighted and Spectroscopic Magnetic Resonance Images

Name of the P.I. : Dr. Bhabesh Deka
Associate Professor
Dept. of ECE, Tezpur University

Sanction Order No. & Date	Grant Sanctioned (₹)	Grant Received (₹)	Details of expenditure incurred Item wise	Amount Rs. (In each head) (₹)
F. No. 8-15/RIFD/ RPS/POLICY-1/ 2016-17, **Date:** 2 August 2017	14,00,000.00	14,00,000.00	**NON-RECURRING** 1. Workstation with Windows 10 Pro, Dell Precision Tower 5810 and Monitor (2 Nos.) 2. P5000 GPU Hardware (2 Nos.)	8,47,770.00
	2,47,059.00	2,22,353.00	**RECURRING** 3. Traveling (for data collection)	6,056.00
			RECURRING 4. Consumables / Stationeries	11,457.00
			Total Rs.:	8,65,283.00

(1) Signature of PI with Seal Associate Professor
Department of Electronic & Comm. Engg.
Tezpur University

(2) Name and Signature of Head of Institution with Seal
Registrar
Tezpur University

(3) 15/9/18

Signature (with Seal) of the Finance Officer/ Auditor/Accounts Officer
(If it is Govt./Govt. Aided Institute)
Finance Officer
Tezpur University
Date:

(4) Signature of Chartered Accountant:
Name of Chartered Accountant: Shekhar Agarwal
Membership No: 310479
Rubber stamp:
Full Address of CA : Tezpur, Assam

Note:-If it is more than one page, each page must be signed & Stamped in all annexure.

FORMAT
For
UTILIZATION CERTIFICATE
(FY 2018 - 19)

Sanction Letter No. 8-15/RIFD/RPS/POLICY-1/2016-17, **Date:** 2 August 2017

A. NON-RECURRING

Sl. No.	Name of the Equipment Procured	Amount Sanctioned (₹)	Amount released (₹)	Amount Utilized (₹)	Unspent Balance (₹)
1	Workstations and GP-GPU Hardware	14,00,000.00	14,00,000.00	13,86,735.00	13,265.00

B. RECURRING

Sl. No.	Name of the Expenses	Amount Sanctioned (₹)	Amount released (₹)	Amount Utilized (₹)	Unspent Balance (₹)
1	Traveling	2,47,059.00	2,22,353.00	18,599.00	1,20,148.00
2	Consumables / Stationeries			83,606.00	
Total		2,47,059.00	2,22,353.00	1,02,205.00	

Certified that the grant has been utilized for the purpose for which it was sanctioned in accordance with the "Terms and Conditions" attached to the grant. If, as a result of check or audit objection some irregularity is noticed at a later stage, action will be taken to refund, adjust or regularize the amount objected to.

Finance Officer (Signature & Seal)
Finance Officer
Tezpur University
Dated: 27/05/19

Registrar/Principal/ Director (Signature & Seal)
Registrar
Tezpur University
Tezpur University
Napaam, Tezpur, Assam-784028

Note: The Utilization Certificate (UC) will be signed by the Registrar/ Finance Officer in the case of Universities, Principals in the case of Colleges and Executive Heads of other Institutions. The Provisional UC may be countersigned by the internal auditors wherever the system of the internal audit exists. In case of the Self Financing/ Private Institutions, UC has to be signed by a Chartered Accountant.

* This is to be submitted every financial year.

Research Promotion Scheme

FORMAT FOR STATEMENT OF EXPENDITURE

(FY 2018-19)

AICTE File No. : 8-15/RIFD/RPS/POLICY-1/2016-17, **Date:** 2 August 2017

Title of the RPS Project : Development of Parallel Processing Embedded Hardware for Super-Resolution of Diffusion Weighted and Spectroscopic Magnetic Resonance Images

Name of the P.I. : Dr. Bhabesh Deka
Associate Professor
Dept. of ECE, Tezpur University

Sanction Order No. & Date	Grant Sanctioned (₹)	Grant Received (₹)	Details of expenditure incurred Item wise	Amount Rs. (In each head) (₹)
F. No. 8-15/RIFD/ RPS/POLICY-1/ 2016-17, **Date:** 2 August 2017	14,00,000.00	14,00,000.00	**NON-RECURRING** 1. Workstation with Windows 10 Pro, Dell Precision Tower 5810 and Monitor (2 Nos.)	8,47,770.00
			2. GP-GPU Hardware	5,38,965.00
	2,47,059.00	2,22,353.00	**RECURRING** 3. Traveling (for data collection)	18,599.00
			RECURRING 4. Consumables / Stationeries	83,606.00
			Total Rs.:	14, 88,940.00

(1) Bhabesh Deka
Signature of PI with Seal
Principal Investigator
AICTE-RPS Project

(2) 7.5.19
Name and Signature of Head of Institution with Seal
Registrar
Tezpur University

(3) 7.5.19
Signature (with Seal) of the Finance Officer/ Auditor/Accounts Officer (If it is Govt./Govt. Aided Institute)
Finance Officer
Tezpur University
Date:

(4) **Signature of Chartered Accountant:**
Name of Chartered Accountant:
Membership No: 310479
Rubber stamp: TEZPUR, ASSAM
Full Address of CA :
Chartered Accountants

Note:-If it is more than one page, each page must be signed & Stamped in all annexure.

FORMAT
For
UTILIZATION CERTIFICATE
(FY 2019 - 20)

Sanction Letter No. 8-15/RIFD/RPS/POLICY-1/2016-17 **Date:** August 2, 2017

A. NON-RECURRING

Sl. No.	Name of the Equipment Procured	Amount Sanctioned (₹)	Amount released (₹)	Amount Utilized (₹)		Unspent Balance (₹)
				(FY2018 - 2019)	(FY2019 - 2020)	
1	Workstations and GP-GPU Hardware	14,00,000.00	14,00,000.00	13,86,735.00	Nil	13,265.00

B. RECURRING

Sl. No.	Name of the Expenses	Amount Sanctioned (₹)	Amount released (₹)	Amount Utilized (₹)		Unspent Balance (₹)
				(FY2018 - 2019)	(FY2019 - 2020)	
1	Traveling	2,47,059.00	2,22,353.00	18,599.00	Nil	
2	Consumables / Stationeries			83,606.00	14,063.00	
Total		2,47,059.00	2,22,353.00	1,02,205.00	14,063.00	1,06,085.00

Certified that the grant has been utilized for the purpose for which it was sanctioned in accordance with the "Terms and Conditions" attached to the grant. If, as a result of check or audit objection some irregularity is noticed at a later stage, action will be taken to refund, adjust or regularize the amount objected to.

Finance Officer
(Signature & Seal)

Dated:

Finance Officer
Tezpur University

Registrar/Principal/ Director
(Signature & Seal)

Tezpur University
Napaam, Tezput, Assam-784028

Registrar
Tezpur University

Note: The Utilization Certificate (UC) will be signed by the Registrar/ Finance Officer in the case of Universities, Principals in the case of Colleges and Executive Heads of other Institutions. The Provisional UC may be countersigned by the internal auditors wherever the system of the internal audit exists. In case of the Self Financing/ Private Institutions, UC has to be signed by a Chartered Accountant.

* This is to be submitted every financial year.

Research Promotion Scheme

FORMAT FOR STATEMENT OF EXPENDITURE

(FY 2019-20)

AICTE File No. : 8-15/RIFD/RPS/POLICY-1/2016-17, **Date:** August 2, 2017

Title of the RPS Project : Development of Parallel Processing Embedded Hardware for Super-Resolution of Diffusion Weighted and Spectroscopic Magnetic Resonance Images

Name of the P.I. : Dr. Bhabesh Deka
Professor
Dept. of ECE, Tezpur University

Sanction Order No. & Date	Grant Sanctioned (₹)	Grant Received (₹)	Details of expenditure Incurred Item wise	Amount Rs. (In each head) (₹)
F. No. 8-15/RIFD/ RPS/POLICY-1/ 2016-17, Date: 2 August 2017	14,00,000.00	14,00,000.00	**NON-RECURRING (2018 - 19)** 1. Workstation with Windows 10 Pro, Dell Precision Tower 5810 and Monitor (2 Nos.)	8,47,770.00
			2. GP-GPU Hardware	5,38,965.00
	2,47,059.00	2,22,353.00	**RECURRING (2018 - 19)** 3. Traveling (for data collection)	18,599.00
			4. Consumables / Stationeries	83,606.00
			RECURRING (2019 - 20) 5. Consumables / Stationeries	14,063.00
			Total Rs.:	15, 03,003.00

(1) Bhabesh Deka

Signature of PI with Seal
Professor
Department of Electronic & Comm. Engg.
Tezpur University

(2) Registrar

Name and Signature of Head of Institution with Seal
Registrar
Tezpur University

(3) 07/9/20

Signature (with Seal) of the Finance Officer/ Auditor/Accounts Officer
(If it is Govt./Govt. Aided Institute)
Finance Officer
Tezpur University

Date:

Agarwal

(4) Signature of Chartered Accountant:
Name of Chartered Accountant:
Membership No:
Rubber stamp:
Full Address of CA :
UDIN- 20310479AAAAQC8814
DATE- 09/10/2020

Note:-If it is more than one page, each page must be signed & Stamped in all annexure.

UTILIZATION CERTIFICATE
(1st April 2020 – 31st Dec 2020)

Sanction Letter No. 8-15/RIFD/RPS/POLICY-1/2016-17 **Date:** August 2, 2017

A. NON-RECURRING

Sl. No.	Name of the Equipment Procured	Amount Sanctioned (₹)	Amount released (₹)	Amount Utilized (₹)	Unspent Balance (₹)
1	Workstations and GP-GPU Hardware	14,00,000.00	14,00,000.00	(FY2018 - 2019) 13,86,735.00	Nil
2	------------------			(FY2019 - 2020) Nil	
3	Macbook Accessories			(1st April 2020 – 31st Dec. 2020) 13,265.00	

B. RECURRING

Sl. No.	Name of the Expenses	Amount Sanctioned (₹)	Amount released (₹)	Amount Utilized (₹)			Unspent Balance (₹)
1	Traveling	2,47,059.00	2,22,353.00	(FY2018 - 2019) 18,599.00	(FY2019 - 2020) Nil	(1st April 2020 – 31st Dec. 2020) Nil	Nil
2	Consumables / Stationeries			83,606.00	14,063	1,06,085.00	
	Total	2,47,059.00	2,22,353.00	1,02,205.00	14,063	1,06,085.00	

Certified that the grant has been utilized for the purpose for which it was sanctioned in accordance with the "Terms and Conditions" attached to the grant. If, as a result of check or audit objection some irregularity is noticed at a later stage, action will be taken to refund, adjust or regularize the amount objected to.

25.2.21

Finance Officer
(Signature & Seal)
Finance Officer
Tezpur University

Dated:

Registrar/Principal/ Director
(Signature & Seal)
Registrar
Tezpur University

Tezpur University
Napaam, Tezpur, Assam-784028

Note: The Utilization Certificate (UC) will be signed by the Registrar/ Finance Officer in the case of Universities, Principals in the case of Colleges and Executive Heads of other Institutions. The Provisional UC may be countersigned by the internal auditors wherever the system of the internal audit exists. In case of the Self Financing/ Private Institutions, UC has to be signed by a Chartered Accountant.

* This is to be submitted every financial year.

Research Promotion Scheme

FORMAT FOR STATEMENT OF EXPENDITURE

(1st April 2020 – 31st Dec 2020)

AICTE File No. : 8-15/RIFD/RPS/POLICY-1/2016-17, **Date:** August 2, 2017

Title of the RPS Project : Development of Parallel Processing Embedded Hardware for Super-Resolution of Diffusion Weighted and Spectroscopic Magnetic Resonance Images

Name of the P.I. : Dr. Bhabesh Deka
Professor, Dept. of ECE, Tezpur University

Sanction Order No. & Date	Grant Sanctioned (₹)	Grant Received (₹)	Details of expenditure incurred item wise	Amount Rs. (in each head) (₹)
F. No. 8-15/RIFD/RPS/POLICY-1/2016-17, **Date:** 2 August 2017	14,00,000.00	14,00,000.00	**NON-RECURRING (2018 - 19)**	
			1. Workstation with Windows 10 Pro, Dell Precision Tower 5810 and Monitor (2 Nos.)	8,47,770.00
			2. GP-GPU Hardware	5,38,965.00
			NON-RECURRING (1st April 2020 – 31st Dec. 2020)	
			3. Macbook Accessories	13,265.00
			RECURRING (2018 - 19)	
			4. Traveling (for data collection)	18,599.00
			5. Consumables / Stationeries	83,606.00
			RECURRING (2019 - 20)	
			6. Consumables / Stationeries	14,063.00
			RECURRING (1st April 2020 – 31st Dec. 2020)	
			7. Consumables/ Stationeries	1,06,085.00
			Total Rs.:	16,22,353.00

(1) Bhabesh Deka
Signature of PI
with Seal
Professor
Department of Electronic & Comm. Engg.
Tezpur University

(2) 26/2/21
Name and Signature of
Head of Institution with Seal
Registrar
Tezpur University

(3) ---------------------------------------
Signature (with Seal) of the Finance Officer/
Auditor/Accounts Officer
(If it is Govt./Govt. Aided Institute)
Finance Officer
Tezpur University

Date: 11/02/2021

(4) Signature of Chartered Accountant:
Name of Chartered Accountant:
Membership No:
Rubber stamp:
Full Address of CA :
UDIN - 21310479AAAAIM2961

Note:-If it is more than one page, each page must be signed & Stamped in all annexure.

Annexure 1

PROJECT COMPLETION REPORT

PROJECT TITLE

Development of Parallel Processing Embedded Hardware for Super-resolution of Diffusion Weighted and Spectroscopic Magnetic Resonance Images

Submitted By

Prof. Bhabesh Deka

Department of Electronics and Communication Engineering

Tezpur University Tezpur - 784 028

Date of Submission

January, 2021

AICTE Ref: F.no. 8-15/RIFD/RPS(Policy-1)/2016-17, Dt: 02/08/2017

Project Duration: From 01.08.2017 to 31.12.2020

Acknowledgements

I am extremely grateful to the All India Council for Technical Education (AICTE), New Delhi, India for selecting our project proposal and providing the required financial support to carry out the project work.

I am highly indebted to the Department of Electronics and Communication Engineering, Tezpur University for giving the opportunity and necessary infrastructures to carry out the project work in the Department.

Prof. Bhabesh Deka

Abstract

Diffusion-weighted magnetic resonance imaging (DW-MRI) and spectroscopic MRI (MRSI) are powerful diagnostic imaging tools as they provide complementary information to that provided by conventional MRI. These images are also acquired at a faster rate, but with low signal-to-noise ratio. This limitation can be overcome by applying image super-resolution techniques. Imaging is done at a low-resolution (LR) as the scanning time for high-resolution (HR) MR images would be very long and not practical besides being expensive for imaging.

This report presents a single-image super-resolution (SISR) technique via sparse representation for DW and MRS images based on non-local total variation (NLTV) approach to regularize an ill-posed inverse problem of SISR. The proposed sparse representation over a learned overcomplete dictionary based SISR technique for DW and MRS images. The proposed SISR method incorporates patch-wise sparsity constraint based on external HR information together with the NLTV as internal information to make the regularization problem more robust.

This report also presents a novel SISR scheme to improve spatial resolution of DW and MRS images. It is based on patch-wise sparse reconstruction of HR patches from LR feature patches utilizing a pair of learned overcomplete dictionaries. Reconstruction not only exploits the sparsity of MR image but also utilize the non-local self-similarity of patches of the input LR image as prior knowledge.

DW-MRI and MRSI along with a synthetic image. Performance evaluations based on different matrices besides visual analysis are carried out to validate and compare the obtained results with the state-of-the-art. It is observed that the proposed method clearly outperforms recent methods in terms of both quantitative and visual analysis. Finally, the proposed algorithm is also implemented using the GP-GPU based parallel hardware along with sequential implementations in order to showcase its potential for real clinical applications.

Contents

List of Tables

List of Figures

CHAPTER 1

Introduction

1.1 Diffusion-weighted imaging (DWI) and spectroscopic magnetic resonance imaging (MRSI)

Diffusion-weighted imaging (DWI) and spectroscopic magnetic resonance imaging (MRSI) are two advanced MR imaging (MRI) techniques. DW images provide information of the internal physiology of an organ by capturing the information of the diffusion of water molecules [2]. Abnormalities can be detected by studying the changes in diffusion pattern from these images. Water molecule diffusion patterns can reveal microscopic details about tissue architecture, either normal or in a diseased state. On the other hand, MRS images provide information of metabolic changes based on chemical composition of tissues. Normal MRI scan may reveal the shape and size of a tumor, while the MRSI provides additional information about the metabolic activity occurring in the tumor [22]. It can be used to monitor bio-chemical changes in tumors, stroke, epilepsy, metabolic disorders, infections, and neuro-degenerative diseases, etc. MRSI also has the same advantage of fast scan time as DWI. In spite of advantages of DWI and MRSI, the rise in the cost of scans and poor signal-to-noise ratio limit their clinical use. These limits can be overcome by image super-resolution (SR) methods [3], which estimate the SR image from one or more observed low-resolution (LR) image(s).

A block diagram of the MR image acquisition system producing LR MR images is shown in Fig. 1.1, which typically possesses various artifacts, like motion blur due to patient movement and breathing; distortions due to magnetic coil field-inhomogeneities and instrumentation noise; downsampling due to poor SNR and

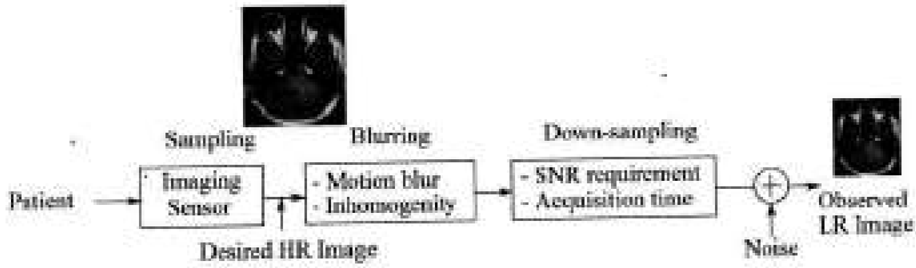

Figure 1.1: Overview of practical MRI image acquisition model [source: [34, Fig. 2]

slow acquisition. We can also describe this acquisition model mathematically by:

$$\mathbf{Y} = SH\mathbf{X} + n, \tag{1.1}$$

where the observed LR image $\mathbf{Y} \in \mathbb{R}^{p \times p}$ is the blurred and downsampled version of the corresponding HR image $\mathbf{X} \in \mathbb{R}^{q \times q}$, H is the blurring operator, S is the downsampling operator and n is the measurement or instrumentation noise. Eq. 1.1 is known as the global imaging model, which is an ill-posed inverse problem as for a given LR image $\mathbf{Y}$, there can be infinitely many choices of $\mathbf{X}$ that would result into the same $\mathbf{Y}$. To regularize the above problem and obtain the best possible or close approximation of $\mathbf{X}$, additional information, like sparsity of image data may be included into the model. Thus, we get a regularized inverse problem as follows:

$$\hat{\mathbf{X}} = \arg\min_{\mathbf{X}} \|SH\mathbf{X} - \mathbf{Y}\|_2^2 + \lambda_1 \Psi_{\text{sparsity}}(\mathbf{X}), \tag{1.2}$$

where Ψ_{sparsity} in the regularization term is an operator on $\mathbf{X}$ that sparsifies the latter. The above model was successfully used for SISR for the first time by Yang *et al.* [43], and recently, in [13] for the SR of MR images, which may be improved further for image SR by putting additional regularizations into it. In the last few decades, many least-square regularization algorithms have been developed for the restoration of high quality images from their corresponding degraded versions [5, 6, 28, 53]. SR methods are categorized as either single-image SR (SISR) or multiple-image SR. SISR is more preferred in MRI as multiple images are difficult to be acquired for the same cross-section, taking considerable scan time. Sparse representation approach has proved to be very effective in case of SISR.

1.2 Related Works

SR method was first applied to MRI by Fiat *et al.* [18]. In the last two decades, SR techniques have been successfully applied to MRI to increase spatial resolution [30, 31]. Generally, based on the number of available input LR images, SR methods are classified into two types. They are namely, the multiple image SR and the single image SR (SISR), respectively. The fundamental idea behind the concept of SR is that information from several sources enrich the overall content of the super-resolved image. The first category of methods refer to the same idea [20, 21]. In the SR of MR images, SISR is preferred to multiple image SR as it is not possible to collect different diffusion or spectroscopic images (captured at different angles, time instants, etc.) of the target field-of-view (FoV) in 2D due to random movement of water molecules present in the tissues. Huang *et al.* [37] first presented a multi-frame image SR technique, where the sub-pixel shifted LR images are generated by using the shifting property of Fourier transform; LR images are then registered into a HR grid through a non-uniform interpolation. The performance of this method is very limited as it does not utilize any sort of *a priori* information. Moreover, it is not very practical due to the problems in acquiring multi-frame LR images [3] of the same scene.

Alternatively, SISR techniques are widely explored that takes only the available single LR image as its input and then generates the target HR version from it. A basic approach of SISR is the image interpolation, e.g. bicubic interpolation or the edge directed interpolation (EDI) as reported in [45], orientation-adaptive interpolation [38], etc., which focus on maximizing the artifact free important information for improved interpolation. However, these methods have the tendency to introduce blurring artifacts and fail to generate high-frequency details during reconstruction. Reconstruction based SR methods using explicit *a priori* information in terms of image gradients is introduced in [36] in order to restrict the solution space of the target HR image for producing the sharp details. These methods are usually time consuming and performances are not good for higher upscale factors. Learning based methods are introduced which can recovet HR image with sharp details within a reasonable computational cost through learning of statistical relationships between the LR and HR images patches from a large training dataset. An example in this category is the work of Freeman *et al.* [19]. They estimated textures and other fine details present in the HR image by modeling natural images using the Markov random field.

Sparse signal recovery using sparse coding theory is successfully applied to SISR techniques for improved performances in various works [13, 23, 26, 29, 32–34, 43, 47]. Yang *et al.* [43] introduces the sparse coding based image super-resolution (ScSR) for generic images by learning joint overcomplete dictionaries from external datasets. Although dictionary based SR methods gives outstanding results, they are relatively slow as the dictionary is to be learnt from a large pool of dataset of similar images or from several patches extracted from the input LR image itself. If the computational cost is not a constraint then sparse coding clearly demonstrates its advantage in terms of higher SNR and better reconstruction quality in the SR of MR image [33]. However, because of severe ill-posed nature of the SR problem, recovered HR images need to be stabilized or re-tuned with better patch consistency approximations. Zhang *et al.* [47] proposed a SISR method that uses a patch-based non-local regularization framework for SR of brain MR image to get more stable output. Shi *et al.* [34] proposed another method using low-rank approximation and total variation (LRTV) which uses both local and global information in MR image to remove blurring artifacts. In [48], authors applied a post-processing method based on sparse derivative prior to remove blurring artifacts for the SR of MR image. Jain *et al.* [23] proposed a patch-wise regularization based spectroscopic MR image SR method that is able to obtain better tissue contrast and structural information compared to the conventional interpolation techniques. Recently, a collaborative sparse representation based regularization with non-local self-similarity (CRNS) is proposed by Chang *et al.* [11], which is able to provide effective recovery of high frequency information and minimum error for the SR of natural images. In another work [10], authors presented a joint SR technique by combining the group-residual-based regularization (GRR) with ridge-regression-based regularization (3R) (JRSR) for better restoration of high frequency details in the SR output. The above study clearly states that the non-local self-similarity (NLSS) within patches of the LR image is highly crucial besides HR information extracted from external datasets and they complement each other for the successful recovery of HR image from the single LR image.

Regularization based SISR methods stabilize the inverse problem of SR by integrating *a priori* information. This ensures that while solving the image reconstruction model, the solution also incorporates a few desired properties of the expected SR output by inducing a *a priori* term, which may be either preservation of edge features based on bilateral total variation, gradient profiles, etc. [27, 39]. These methods require iterative implementation and suffer from slow convergence and high computational costs. Most of the methods in this category fail to remove the high-frequency noise or blurring, while simultaneously preserving the edges or other details. Others change the image contrast during SR image reconstruction and provides inadequate visual quality for higher upscale ratios. On other hand, learning based SISR methods have become the most popular among the state-of-the-art. These methods involve a training stage to learn the relationship between LR and HR examples and the same information is utilized as regularization during reconstruction. There are different learning schemes, like example learning [19], self-learning [44], dictionary learning [43], etc. Recently, the dictionary learning based approach along with sparse representation has attracted the highest attention from the SR research community due to its high accuracy. With the continuing effort for the development of better ℓ_1-minimization tools and dictionary learning strategies, such SR algorithms have the flexibility for incorporating better regularization schemes for better and stable results [10, 25].

Recently, the non-local self-similarity (NLSS) has been used in the restoration of fine details and textures of natural images [40, 54]. This is based on the fact that these images contain several patches or regions in the entire image, which are similar but may not be connected in the image. In several works, the non-local means (NLM) [50] and the non-local total variation (NLTV) [32] based regularizations are applied to incorporate information of the local statics during sparse reconstruction of HR patches. Non-local low-rank regularization (NLR) has been introduced in [15] that considers a matrix of the non-local similar patches and performs low-rank minimization of it to enhance non-local similarity among the reconstructed HR patches. Authors in [46] effectively applied NLR besides collaborative representation based regularization for the SR of natural images with state-of-the-art results.

1.3 Motivation of the Work

SISR is more preferable in medical imaging as multiple images are difficult to be acquired in a particular cross-section, taking considerable scan time. Sparse representation approach has proved to be very effective in case of single-image SR. But the stabilization for the solution of inverse problems is a major issue in sparsity approach, which can be overcome by regularization.

SISR is more preferred in MRI as multiple images are difficult to be acquired for the same cross-section, taking considerable scan time. Sparse representation approach has proved to be very effective in case of SISR. The general idea behind sparse representation based image SR is that an overcomplete dictionary is first learnt from an external HR database, which is then explored for inducing HR information in the reconstructed image via a sparsity regularization approach. Together with a robust dictionary learning, the stabilization of the solution from sparse representation is a major concern in this approach, which can be overcome satisfactorily by incorporating relevant *a priori* information into the reconstruction model.

SR problem is highly ill-posed in nature and methods applying the sparse coding theory tries to impose prior knowledge in order to regularize it optimally. In this context, sparse representation based SR problem can be made more robust and effective by putting more effort in integrating more relevant information into the model. Furthermore, quality of reconstructed images may also be improved by using overcomplete dictionaries learnt from example image patches containing significant high frequency features in it at varying levels of upscaling. Moreover, in order to make the computational cost of the SR algorithm clinically relevant for MRI, we can adopt a hybrid computing environment, where more complex and intensive mathematical operations may be carried out in parallel and less significant and routine mathematical operations may be implemented in serial. Most of the work reported in the literature either uses learned dictionary which act as a source of external information to enhance resolution of the target LR image [23, 26, 33, 43].

1.4 Major Contributions

The major contribution of this report are as follows:

- ▷ To develop a SISR method for MR images using sparse representation along with non-local total variation (NLTV) regularization.
- ▷ A novel MR image feature extraction technique is developed to extract the most relevant features for accurate SR of clinical DW and MRS images using the morphological component analysis (MCA) and second order high-pass filter.
- ▷ A global dictionary learning method is proposed using the K-singular value decomposition (K-SVD) technique with the orthogonal matching pursuit (OMP) algorithm as the sparse coder.
- ▷ A patch-wise sparse reconstruction problem is modeled for HR image reconstruction; Sparse optimization problem is solved by an efficient sparse coding method.
- ▷ Sparse representation based coupled overcomplete dictionaries are learnt using DW and MRS images and utilized them to extract *a priori* HR information for the reconstructed patches from external datasets.

- ▷ Non-local low-rank based regularization is incorporated in the reconstruction model to exploit self-similarity of LR pathes from the input image for preserving sharp edges and fine details besides smooth regions since MR image is naturally piece-wise smooth and contain repetitive patterns throughout the image. We use it as an additional *internal prior* in the proposed model.

- ▷ Proposed a composite sparse reconstruction model consisting of both the regularizing priors- external and internal as mentioned above. Two subproblems are then solved iteratively by using the alternating direction method of multipliers (ADMM) algorithm. Extensive simulations are carried out with different clinical DWI and MRSI datasets for different upscale factors and compared results with the state-of-the-art.

- ▷ Implemented the proposed SISR algorithm in a hybrid CPU-GPU environment for different multi-slice DWI and MRSI datasets to demonstrate its potential for parallel implementation.

1.5 Organization of the Report

The rest of this report is organized as follows: in chapter 2, a Sparse Representation based Super-resolution of MRI Images with Non-Local Total Variation Regularization is presented. Chapter 3 describes the proposed methodology of Sparse Representation over a Learned Overcomplete Dictionary based Super-resolution Technique for DW and MRS Images. Chapter 4 describes the proposed methodology of Diffusion-weighted and Spectroscopic MRI Super-resolution using Sparse Representations. Finally, a brief conclusion is provided in chapter 5.

CHAPTER 2

Sparse Representation based Super-resolution of MR Images with Non-Local Total Variation Regularization

The performances of sparse representation algorithms for image SR are related to several phenomenons, like, quality of the dictionary trained, effectiveness of the constraint term selected for regularization, etc. The proposed method for SR reconstruction from a set of LR MR images is discussed in the following sections. It consist of two parts: first, learning of LR and HR dictionaries and second, reconstruction of HR output image utilizing the learned dictionaries. The reconstruction algorithm is again can be divided into the following sub-tasks: first, extraction of high-frequency features of the patches,then solving a sparse prior based regularization and secondly, a non-local total variation regularization to restore the textural details.remove the undesirable staircase artifact to recover the fine details and textures. Finally, a global image regularization is done that helps in incorporating the given LR image's point spread function into the reconstructed HR images by utilizing the image acquisition model constraint.

2.1 Sparsity based Image Super-resolution

In the beginning, overlapping patches of size $k \times k$ are extracted from the input LR image Y. The sparse coefficients α corresponding to each low-resolution patch y is found with respect to the trained dictionaries D_l and D_h. Next, these sparse coefficients are combined with high-resolution dictionary D_h to find high-resolution patches x.

The solution of the following sparse regularization problem gives the sparse coefficients corresponding to each low-resolution patch y:

$$\alpha^{*} = \arg\min_{\alpha} \left\| D'\alpha - \tilde{y} \right\|_2^2 + \lambda \left\|\alpha\right\|_1, \tag{2.1}$$

where $D' = \begin{bmatrix} D_\ell \\ TD_h \end{bmatrix}$, $\tilde{y} = \begin{bmatrix} y \\ w \end{bmatrix}$, and λ is the regularization parameter. T is the overlap region extraction operator which finds the region which is common to both the presently reconstructing patch and the latest HR patch generated; w represents the overlapped pixels contained in the previously reconstructed HR image.

Following the computation of sparse coefficients α^{*} using Eqn. 2.1, HR patches x are obtained by solving the following relation which supports the fact that the HR and LR dictionaries shares the same sparse representation.

$$x \approx D_h\alpha^{*} \tag{2.2}$$

Arranging all the individual HR patches reconstructed by Eqn. 2.2 on a single grid will yield to an intermediate HR image X_0. Before finding the initial HR reconstructed image X_0 by the minimization problem, non local total variation regularization is performed so that the patches to be reconstructed fit properly in the above minimization formulation. Again due to measurement errors, X_0 may not fit the generalized model, $Y = WX$, where Y is the input LR image, X is the desired HR image and W is the image sampling operator. For overcoming these limitations due to noise, a global reconstruction constraint is imposed by solving a minimization problem:

$$X^{*} = \arg\min_{X} \|WX - Y\|_2^2 + \lambda\|X - X_0\|_2^2 \tag{2.3}$$

The above equation 4 is the gradient descent method, which is minimized iteratively to find the final reconstructed image X_0.

2.2 NLTV Regularization

The non-local means (NLM) filtering implies the weighted average of the surrounding pixels within a search window for the computation of the new filtered pixel value. Two blocks of the HR image X_0 having central pixels at x_i and x_j contributes to weight w_{ij} which is the gaussian distance l_2 between the blocks [49]. Consider x_i and x_j denote the pixel at the center of $b_s \times b_s$ blocks and it is assumed that x_j lies in the search window of x_i. Weight w_{ij} is computed by:

$$w_{ij} = \exp(-||x_j - x_i||_2^2/f^2)/c_i \tag{2.4}$$

where f and c_i are controlling parameter and normalization factors, respectively. The new filtered pixel value is denoted by NLM (x_i), and this approach of filtering has lead to a new approach of regularization, known as nonlocal regularization. Consider all the pixels in the center organized as a column vector, represented as r and all the weights are also organized as column vector, represented as w. Mathematically, this nonlocal regularization can be represented as:

$$\sum_{x_i \in x} ||x_i - w_i^T r_i||_2^2 \tag{2.5}$$

These weights are updated iteratively and before the implementation of gradient descent method for final reconstruction, the nonlocal total variation (NLTV) regularization is implemented, the formulation of this approach is as:

$$\min_x ||D_h \alpha|| + \alpha||x - Wx||_2^2 \tag{2.6}$$

The solution of the above formulation is the basis of the NLTV regularization. The HR image X_0 obtained after the regularization is used in equation 4, which undergoes minimization iteratively to obtain the final SR image X^*.

2.3 Dictionary Learning

Two training image patch pairs, set of high-resolution patches is represented by $X^h = x_1, x_2, ..., x_k$ and set of low-resolution patches is represented by $Y^l = y_1, y_2, ..., y_k$. These two dictionaries are jointly trained with the condition that both HR and LR image patches have a common sparse representations among them. A joint sparse representation regularization can be formulated involving the LR and HR image patches simultaneously. Mathematically,

$$\min_{\{D_h, D_l, Z\}} \frac{1}{R}||X^h - D_h Z||_2^2 + \frac{1}{S}||Y^l - D_l Z||_2^2 + \lambda(\frac{1}{R} + \frac{1}{S})||Z||_1 \qquad (2.7)$$

where LR and HR patches in vector form have dimensions S and R respectively. $||Z||_1$ is a ℓ_1-norm term that enforces sparsity into both the dictionaries. Eqn. 2.7 is solved iteratively for three parameters simultaneously to obtain the HR and LR dictionaries D_h and D_l.

2.4 Results and Discussion

Simulations of the proposed work is carried out using MATLAB (R2015b) environment on PC having configurations as follows: OS- Windows 7, Processor: Intel core i5 (2.2 GHz), and RAM: 8 GB. The diffusion-weighted MRI data has been acquired from a GE HDx 1.5T with the following parameters: TR/TE: 4225/76.6 ms; Slice thickness: 5 mm, spacing between scans: 5 mm; Field of view (FOV): 100 × 100; Flip angle: 90^0. The spectroscopic MRI images have also been acquired from a GE HDx 1.5T with the following parameters: TR/TE: 150/1.372 ms; Slice thickness: 8 mm; spacing between scans: 5 mm; Field of view (FOV): 100 × 100; Flip angle: 70^0.

Table 2.1: Quantitative evaluations of the DW image SR for different methods using upscale 2 and 3

Parameters	Upscale Factor 2				Upscale Factor 3			
	BCI	LRTV	ScSR	Proposed	BCI	LRTV	ScSR	Proposed
MSE	28.36	78.92	22.49	**17.79**	41.36	130.33	24.06	**16.41**
MSSIM	0.974	0.883	0.977	**0.982**	0.951	0.872	0.962	**0.971**
PSNR (dB)	34.89	28.12	35.92	**36.93**	33.27	28.29	35.62	**36.98**
MI	3.88	1.46	3.89	**4.11**	2.897	4.01	**4.15**	3.517

Table 2.2: Quantitative evaluations of the spectroscopic image SR for different methods using upscale 2 and 3

Parameters	Upscale Factor 2				Upscale factor 3			
	BCI	LRTV	ScSR	Proposed	BCI	LRTV	ScSR	Proposed
MSE	24.98	44.09	14.32	**11.66**	41.36	130.33	24.06	**16.41**
MSSIM	0.966	0.878	0.976	**0.980**	0.954	0.798	0.965	**0.972**
PSNR (dB)	35.44	32.99	37.91	**38.92**	35.67	29.29	37.73	**38.67**
MI	3.517	2.568	3.726	**3.827**	3.521	2.327	3.661	**3.789**

2.4.1 Simulations

First, the LR dictionary D_l and the HR dictionary D_h are trained jointly where both consist of 512 atoms in each. For training, a number of 1,00,000 LR/HR patch pairs are selected from about 30 standard MR images. The regularization parameter for the dictionary has been considered as $\lambda = 0.15$. This dictionary has been trained as per the approach proposed by Yang *et al.* [43].

Next, for the super-resolution reconstruction, two upscale factors have been considered, i.e., 2 and 3. For both the upscale factors, size of the LR input is 128×128. Size of the output HR image is 256×256 and 384×384 for upscale factor 2 and 3 respectively. The results of the proposed method and some other SR based methods has been given with their magnified view. In Tables 1-2, DWI results represent the SR results of diffusion-weighted MRI images and MRSI results represent the SR results of Spectroscopic MRI images.

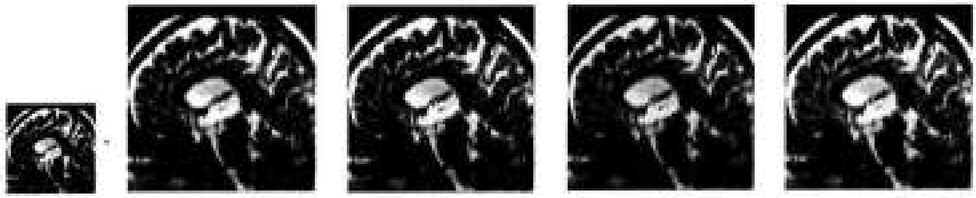

Figure 2.1: Results of DW MRI by using different SR techniques for upscale factor 2

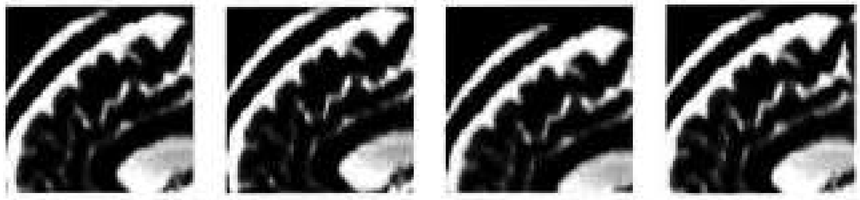

Figure 2.2: Magnified view of results of DW image SR for upscale factor 2

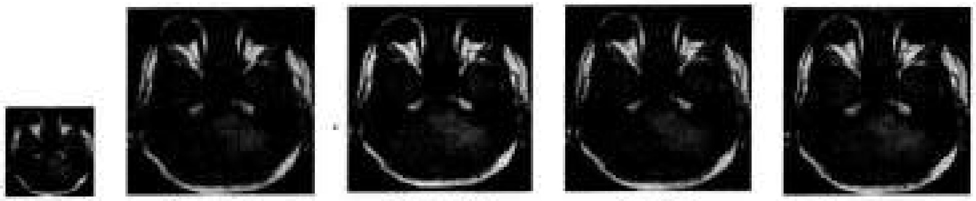

Figure 2.3: Results of spectroscopic image SR by different techniques for upscale factor 2

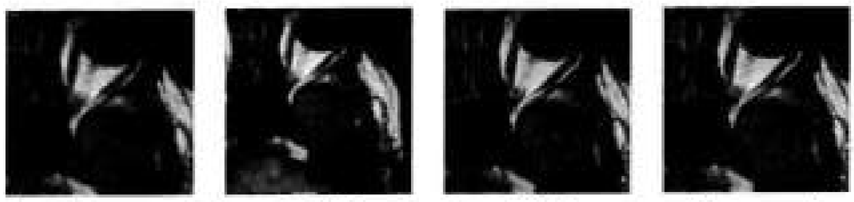

Figure 2.4: Magnified view of results of spectroscopic image SR for upscale factor 2

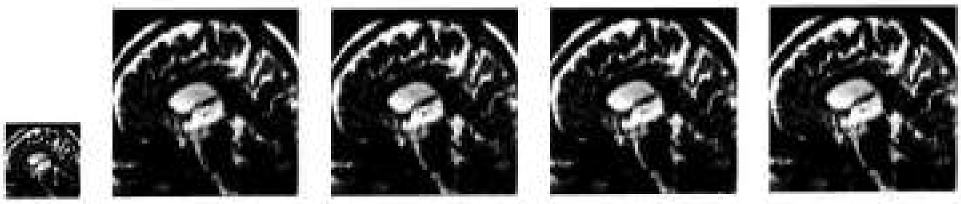

Figure 2.5: Results of DW MR image SR by different techniques for upscale factor 3

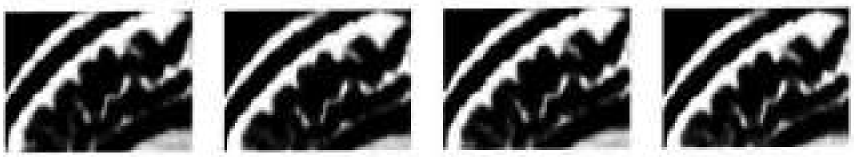

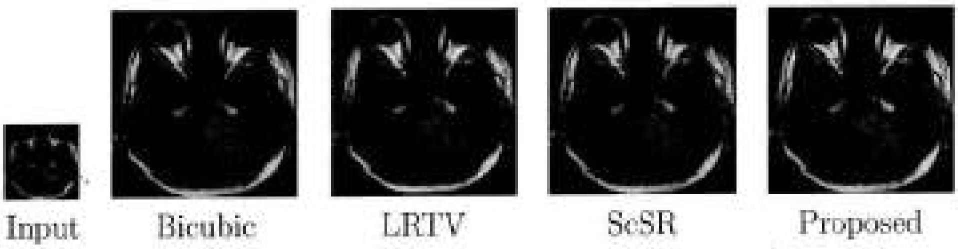

Figure 2.7: Results of spectroscopic image SR by different techniques for upscale factor 3

Figure 2.8: Magnified view of results of Spectroscopic image SR for upscale factor 3

2.4.2 Evaluations

The simulation results obtained are evaluated both visually and quantitatively. In Figs. 1-8, it is clearly seen that the fine details such as edges have been preserved efficiently in the proposed method. From Tables 1-2, it can be seen that evaluation parameters obtained for the proposed method are better in terms of peak signal-to-noise ratio (PSNR) as well as mean structural similarity index (MSSIM) compared to the traditional bicubic interpolation techniques. The proposed method has also shown better results as compared to ScSR proposed by Yang *et.al.* [43] and LRTV proposed in [34]. Compared to the ground truth, bi-cubic interpolation, and LRTV methods produce blurry results. As far as ScSR is concerned, it does not produce blurring artifacts, but in comparison to the proposed method, it it does not preserve equivalent edge details. We have compared the image quality using two more metrics mean-square error (MSE) and mutual information (MI) [8] between the ground truth and the SR result image. For better image quality, MSE should be less and MI should be more. All the images used in the experiments are brain images. The magnified views of the results clearly show the zoomed view of a specified portion of the results. It can be seen that fine details are recovered by the proposed method.

2.5 Conclusions

In this chapter, we have shown that the implementation of non-local TV regularization for solving the regularization issues of the sparsity based approach can be a viable solution to the issues. This combination provides better consistency of patches, thereby giving better results. Quantitative comparisons show that the proposed method outperforms the existing regularization based approaches. Proposed method is computationally expensive due to the iterative process of regularization. As a future work, this can be extended to multi-core processing for computationally efficient results.

CHAPTER 3

Sparse Representation over a Learned Overcomplete Dictionary based Super-resolution Technique for DW and MRS Images

In this chapter, the development of a sparse representation based MR image SR algorithm using coupled overcomplete dictionary training along with a non-local total variation (NLTV) regularization for obtaining the most stable and accurate output. The proposed MR image SR method is divided into three phases, namely, *Feature Extraction, Coupled Dictionary Training* and *SR Reconstruction*. The procedure to carry out these tasks are explained in the following subsections.

3.1 Feature Extraction

The training dataset $\mathbf{X}_C$ for dictionary learning is collected from sample patches taken from LR and HR training images. Here, the HR patch vector $\mathbf{X}_h \in \Re^{m\times P}$ consists of $\sqrt{m} \times \sqrt{m}$ size patches extracted directly from some available HR MR images similar to the LR images, where P is the total number of such patches. On the other hand, LR patch vector is not directly obtained from LR patches, but acquired from feature enriched LR patches. This is achieved by first carrying out a feature extraction procedure before LR patch formation. In the proposed method, feature extraction is performed using the morphological component analysis (MCA) reported in [16] and high-pass filtering of first- and second-orders. MCA gives texture and cartoon layers from the given LR image. For example, as shown in Fig. 3.1, the separated texture image includes all the high-frequency information, while the cartoon image just gives the structural overview of the actual image.

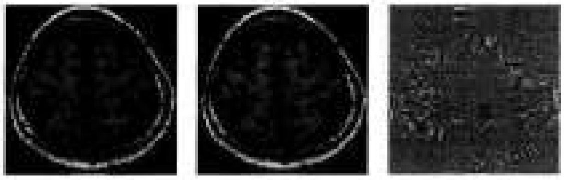

(a) original (b) cartoon (c) texture

Figure 3.1: Example of MCA decomposition for texture image extraction [16]

In order to decompose the LR image $\mathbf{X}_\ell$ into its texture $(\mathbf{X}_\ell)_t$ and cartoon $(\mathbf{X}_\ell)_c$ layers. The MCA obtains sparse representation of each layer by a given dictionary. The dictionary is built as a set of dictionaries related to multiscale transforms, such wavelets, ridgelets, or curvelets. For texture image separation, the DCT and curvelet transforms are chosen which gives better edge description. Mathematically,

$$\mathbf{X}_\ell = (\mathbf{X}_\ell)_t + (\mathbf{X}_\ell)_c = \mathbf{D}_t\boldsymbol{\alpha}_t + \mathbf{D}_c\boldsymbol{\alpha}_c, \tag{3.1}$$

where $\mathbf{D}_t$ and $\mathbf{D}_c$ are the dictionaries for texture and cartoon layers, respectively, while $\boldsymbol{\alpha}_t$ and $\boldsymbol{\alpha}_c$ are the corresponding sparse coefficients vectors. To perform texture image extraction from a noisy image, Eq. 3.1 is modeled as a basis pursuit (BP) based regularization problem, where the decomposition performs approximation of the image layers, leaving some error to be absorbed by content that is not represented well by both dictionaries. Moreover, another penalty term based on total variation (TV) is added into the unconstrained regularization problem to recover smooth targets with sharp edges from the cartoon image. The overall decomposition problem is mathematically expressed as follows:

$$\begin{gathered}\{\boldsymbol{\alpha}_t^{opt}, \boldsymbol{\alpha}_c^{opt}\} = \underset{\{\boldsymbol{\alpha}_t,\, \boldsymbol{\alpha}_c\}}{\arg\min} \|\boldsymbol{\alpha}_t\|_1 + \|\boldsymbol{\alpha}_c\|_1 + \\ \lambda \|\mathbf{X}_\ell - \mathbf{D}_t\boldsymbol{\alpha}_t - \mathbf{D}_c\boldsymbol{\alpha}_c\|_2^2 + \lambda TV\{\mathbf{D}_c\boldsymbol{\alpha}_c\}\end{gathered} \tag{3.2}$$

The above optimization problem is solved using the block-coordinate-relaxation method [4]. In the proposed method, the texture component, $(\mathbf{X}_\ell)_t$ will be considered for LR dictionary training as it mainly contains the high-frequency attributes. Furthermore, we apply four 1-D derivative filters of orders 1 and 2 as reported in [43] on $(\mathbf{X}_\ell)_t$ for extracting the horizontal and vertical features for dictionary training.

The filtered outputs give rise to four separate gradient maps.

Next, we select patches from these gradient maps for learning the LR dictionary. For each patch index (depending on the number of overlapping pixels, the total number of indices will vary), we obtain four feature patches, one from each of the gradient map. These four feature patches are then concatenated to form the single feature vector of dimension $4m \times 1$. The process is repeated for remaining patch locations as well. In this way, we build a training dataset of size $4m \times P$ for the LR dictionary.

3.2 Coupled Dictionary Training

The feature extraction stage makes the sparse representation more effective by considering only the high-frequency information contained in the LR image and avoiding any redundant content. Now, a joint sparse regularization problem is formulated to learn the coupled overcomplete dictionary $\mathbf{D}_C$ from the combined dataset $\mathbf{X}_C = \left[\mathbf{X}_h \in \Re^{m \times P}; \mathbf{X}_{\ell_{(\mathrm{feature})}} \in \Re^{4m \times P}\right]$. Assuming a common sparse coding vector $\mathbf{Z}$ from both HR and LR feature patches, the joint dictionary training may be formulated as the following minimization problem [42]:

$$\min_{\{\mathbf{D}_h, \mathbf{D}_\ell, \mathbf{Z}\}} \frac{1}{R}||\mathbf{X}_h - \mathbf{D}_h\mathbf{Z}||_2^2 + \frac{1}{S}||\mathbf{X}_{\ell_{(\mathrm{feature})}} - \mathbf{D}_\ell\mathbf{Z}||_2^2 + \lambda(\frac{1}{R} + \frac{1}{S})||\mathbf{Z}||_1, \tag{3.3}$$

where R and S represent dimensions of HR and LR feature patches in vector form, and λ represents the regularization parameter. Above problem may also be simplified by formulating an equivalent problem of learning a combined dictionary i.e. the coupled dictionary $\mathbf{D}_C = [\mathbf{D}_h; \mathbf{D}_\ell]$ as follows:

$$\min_{\{\mathbf{D}_C, \mathbf{Z}\}} ||\mathbf{X}_C - \mathbf{D}_C\mathbf{Z}||_2^2 + \lambda(\frac{1}{R} + \frac{1}{S})||\mathbf{Z}||_1. \tag{3.4}$$

Eq. 3.4 can be solved by using the K-SVD [1] algorithm. A pictorial representation of the proposed coupled dictionary training scheme is shown in Fig. 4.1

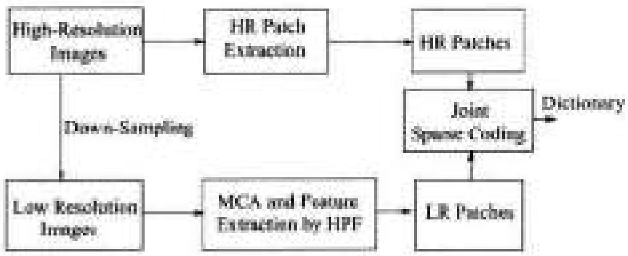

Figure 3.2: Proposed dictionary training method

3.3 Sparsity and NLTV regularization based SR Image Reconstruction

Sparsity Regularization

In reconstruction phase, MCA decomposition is first applied on the test LR image $\mathbf{Y}$ to get its texture and structure (cartoon) components, $\mathbf{Y}_t$ and $\mathbf{Y}_c$, respectively. $\mathbf{Y}_t$ is then upscaled by bicubic interpolation and feature patches are extracted from it. These LR feature patches are used for sparse reconstruction of their corresponding HR patches. Mathematically, the patchwise sparse representation problem using interpolated LR feature patches is given by:

$$\hat{\boldsymbol{\alpha}} = \arg\min_{\boldsymbol{\alpha}} \left\| \tilde{\mathbf{y}} - \tilde{\mathbf{D}}\boldsymbol{\alpha} \right\|_2^2 + \lambda_1 \left\| \boldsymbol{\alpha} \right\|_1, \tag{3.5}$$

where $\tilde{\mathbf{y}} = \begin{bmatrix} \mathbf{y} \\ w \end{bmatrix}$, $\tilde{\mathbf{D}} = \begin{bmatrix} \mathbf{D}_\ell \\ T\mathrm{D}_h \end{bmatrix}$, T is an operator that extracts the region of overlap between the current reconstructed patch with the most recently reconstructed HR patch, while w representing the overlapped pixels, and λ_1 is the regularization parameter. Eq. 3.5 is a convex optimization problem, which is efficiently solved by the sparse coding algorithm [25] that gives superior performance over classical ℓ_1-minimization tools. Next, the corresponding HR patches $\mathbf{x}$ are obtained as follows:

$$\mathbf{x} = \mathbf{D}_h\hat{\boldsymbol{\alpha}}. \tag{3.6}$$

After obtaining all the HR patches as above, they are stitched together to form an approximate full texture image $\mathbf{X}_t^0$, which is added to the bicubic interpolated cartoon component $\mathbf{X}_c^{hi}$ to obtain the intermediate HR image $\mathbf{X}^0$.

NLTV Regularization

The non-local means (NLM) filtering implies the weighted average of the surrounding pixels within a search window for the computation of the new filtered pixel value. Two blocks of the HR image $\mathbf{X}^0$ having central pixels at x_i and x_j contributes to weight w_{ij}, which is the Gaussian distance or the ℓ_2-norm distance between the two blocks [49]. Consider x_i and x_j denote the pixels at the center of $b_s \times b_s$ blocks: $\mathbf{x}_i$, $\mathbf{x}_j$, and it is assumed that x_j lies in the search window of x_i. Weight w_{ij} is computed by:

$$w_{ij} = \exp(-\|\mathbf{x}_j - \mathbf{x}_i\|_2^2/f^2)/c_i, \tag{3.7}$$

where f and c_i are controlling parameter and normalization factors, respectively. The new filtered pixel value is denoted by NLM (x_i), and this approach of filtering has lead to a new approach of regularization, known as nonlocal regularization. Consider all the pixels around x_i within the search window organized as a column vector, represented as $\mathbf{r}_i$ and corresponding weights organized as column vector, represented as $\mathbf{w}_i$. Mathematically, this nonlocal regularization can be represented as:

$$\sum_{x_i \in \mathbf{x}} ||x_i - \mathbf{w}_i^T \mathbf{r}_i||_2^2. \tag{3.8}$$

These weights are updated iteratively and before the implementation of gradient descent method for final reconstruction, the nonlocal total variation (NLTV) regularization is implemented, the formulation of this approach is as:

$$\min_{\mathbf{X}^0} \mathrm{TV}(\mathbf{X}^0) + \lambda_2 ||\mathbf{X}^0 - \mathbf{W}\mathbf{X}^0||_2^2, \tag{3.9}$$

where λ_2 is the regularization parameter. The solution of the above formulation is the basis of the NLTV regularization. The HR image $\mathbf{X}^0$ obtained after the NLTV regularization is used to reconstruct the final SR image $\mathbf{X}^*$.

To avoid the patch inconsistency problem and to satisfy the image acquisition model, a back-projection step is carried out by imposing a global reconstruction constraint as follows:

$$\mathbf{X}^{*} = \arg\min_{\mathbf{X}} ||SH\mathbf{X} - \mathbf{Y}||_2^2 + \lambda_3||\mathbf{X} - \mathbf{X}^0||_2^2, \tag{3.10}$$

where λ_3 is the regularization parameter. Above equation is the least-square problem having a closed form solution and solved by the gradient descent algorithm. We summarize the proposed algorithmic steps in Algorithm 1.

Algorithm 1 : Super-resolution Reconstruction

Input: input image $\mathbf{Y}$, dictionaries $\mathbf{D}_\ell$ and $\mathbf{D}_h$

MCA decomposition: $\mathbf{Y} \rightarrow \mathbf{Y}_c, \mathbf{Y}_t$
$\mathbf{X}_c^{bi} \Leftarrow$ Bicubic interpolation of $\mathbf{Y}_c$
for each $\sqrt{m} \times \sqrt{m}$ patch $\mathbf{y}_t$ in $\mathbf{Y}_t$ **do**
    $xx \leftarrow$ patch indexes in x-dimension
    $yy \leftarrow$ patch indexes in y-dimension
    for (int $xx = 0; xx < rows; xx^{++}$) **do**
        for (int $yy = 0; yy < cols; yy^{++}$) **do**
            $\boldsymbol{\alpha}^{*} = \min_{\boldsymbol{\alpha}} ||\tilde{\mathbf{D}}\boldsymbol{\alpha} - \tilde{\mathbf{y}}||_2^2 + \lambda||\boldsymbol{\alpha}||_1$
        end for
    end for
    for each HR patch $\mathbf{x}_{t_i}$ **do**
        $\mathbf{x}_{t_i} \leftarrow \mathbf{D}_h\boldsymbol{\alpha}^{*}$;
    end for
end for
for intermediate HR image **do**
    $\mathbf{X}^0 \Leftarrow \mathbf{X}_c^{bi} + \mathbf{X}_t^0$
end for
TV regularization: NLTV $\{\mathbf{X}^0\}$
for (int $i = 0; i <$ (maxIter); $i++$) **do**
    $\mathbf{X}^{*} = \arg\min_{\mathbf{X}} ||SH\mathbf{X} - \mathbf{Y}||_2^2 + \lambda\,||\mathbf{X} - \mathbf{X}^0||_2^2$
end for

Output: super-resolved image $\mathbf{X}^{*}$

3.4 Results And Discussion

The detailed experimental setup and simulations carried out in this work are discussed in following.

3.4.1 Simulation Setup

Database Preparation

Two types of clinical MR images are collected from two local Hospitals, namely, Apollo Hospitals, Guwahati and GNRC, Six mile, Guwahati. First, the DW images are acquired using scanners- GE 1.5 T SIGNA Explorer with following parameter settings: scanning sequence: GR, matrix size: 256×256, TR/TE: 47.5 msec./ 2.6 msec., slice thickness: 5 mm, no. of averages: 1, and GE 1.5 T SIGNA HDxt with scanning sequence: EP/SE, matrix size: 256 256, TR/TE: 4225 msec./ 77.9 msec., slice thickness: 5 mm, no. of averages: 2. On the other hand MRS images are acquired using a GE 1.5 T SIGNA Explorer with following parameter settings: scanning 4sequence: EP/SE, matrix size: 256×256, TR/TE: 4313 msec./85.2 msec., slice thickness: 5 mm, no. of averages: 1.

For dictionary training, we prepare two separate databases for DW and MRS images, each consisting of 25-35 high quality images. Experiments are conducted assuming these images as representatives of some HR images, corresponding LR versions are obtained by blurring and downsampling operations as discussed in Section 1. On the other hand, for testing of the proposed algorithm, two sample DW and MRS images are considered, which are not included in the training database.

Simulation Environment

All simulations are carried out in the MATLAB (R2017a) environment on a workstation having specifications as follows: Intel(R) Xeon(R) CPU E5-2650 v4 @ 2.20 GHz, 2201 MHz and 12 Cores; GPGPU: NVIDIA Quadro P5000 with 16 GB GDDR5X memory and 2560 CUDA cores.

Evaluation Parameters

Four reference based quantitative metrics are considered for the performance evaluation of SR reconstructed images using the proposed algorithm. They are, peak signal-to-noise ratio (PSNR), structural similarity index (SSIM), feature similarity (FSIM) [53] and mutual information (MI) [9]. A high value of PSNR and SSIM indicates better reconstruction quality. FSIM is specially used for MRI images that quantifies local image quality through gradient magnitude similarity calculation and falls in the range [0, 1]. Similarly, MI is a measure of the degree of statistical dependence between two random variables. Both FSIM and MI increase for better image quality.

3.4.2 Simulations

Dictionary Training

In this experiment, two pair of coupled overcomplete dictionaries are trained, both for MRSI and DWI images by using K-SVD based learning approach [1]. First, 100000 number of HR and LR sample patch-pairs are prepared from the training datasets. Next, to assure that most significant feature patches are selected in the training patch vector, we apply a pruning operation on it where the patches with a less variance is discarded. This in turn produce a final training dataset with the most significant patch-pairs for dictionary learning.

As depicted in Fig. 4.1, the HR dictionary is trained on the HR image patches while the LR dictionary is trained on features extracted from the LR training images. In this experiment, for SR by factor 2, both LR and HR patch size is considered as 5×5. A dictionary with 256 atoms is learnt with each atom having a size of 25×1 for $\mathbf{D}_h$ and 100×1 for the $\mathbf{D}_l$. On the other hand, for SR by factor 3, the LR image is first upscaled by 2 using bicubic interpolation and then 6×6 (which is 2 times the original 3×3 LR patch) LR patches are extracted with 1 pixel overlap. The corresponding HR patches are of size 9×9 having 3 pixel overlaps. Consequently, for upscaling by 3, the $\mathbf{D}_h$ and $\mathbf{D}_l$ are of sizes 81×256 and 144×256, respectively.

Results

In this work, four MR images, namely, MRSI1 (resolution: 424 × 360), MRSI2 (resolution: 465 × 390), DWI1 (resolution: 172 × 142) and DWI2 (resolution: 189 × 153) are taken as the original HR images. Then a LR test image is generated from

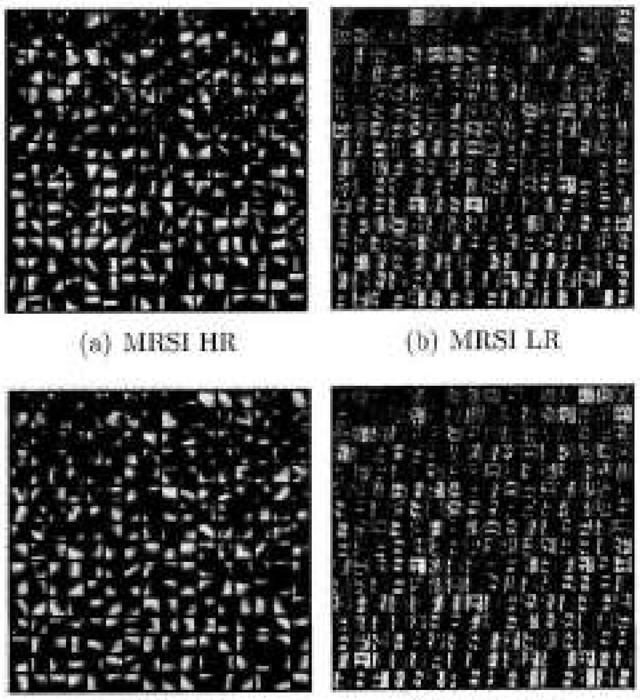

(a) MRSI HR (b) MRSI LR

(c) DWI HR (d) DWI LR

Figure 3.3: HR and LR dictionary images trained from MRSI and DWI training datasets respectively

each of them by applying blurring and downsampling operations. We use a Gaussian blur kernel of size 5×5 and standard deviation value $\sigma = 0.5$. For MRSI1 and DWI1, the downsampling ratio is 2 while that of MRSI2 and DWI2 is 3. So, LR image sizes for MRSI1, MRSI2, DWI1 and DWI2 become 212×180, 155×130, 172×142 and 63×51, respectively.

Simulation results are evaluated both visually and quantitatively on DW and MRS images for different upscale ratios. Tables 1-2 show evaluation of different performance metrics for different state-of-the-art SR methods along with the proposed method. It can be seen that the proposed method outperforms both in terms of PSNR as well as SSIM compared to others. The proposed method has shown better results as compared to the ScSR proposed by Yang *et.al.* [43], LRTV [35] and JRSR [10]. In terms of PSNR, the proposed method, on an average, shows an improvement of approximately 2 dB than SCSR for 2x zooming of a test MRS image, while the same is approximately 0.8 dB for 3x zooming for another test MRS image. When compared to the JRSR, the proposed method on an average shows

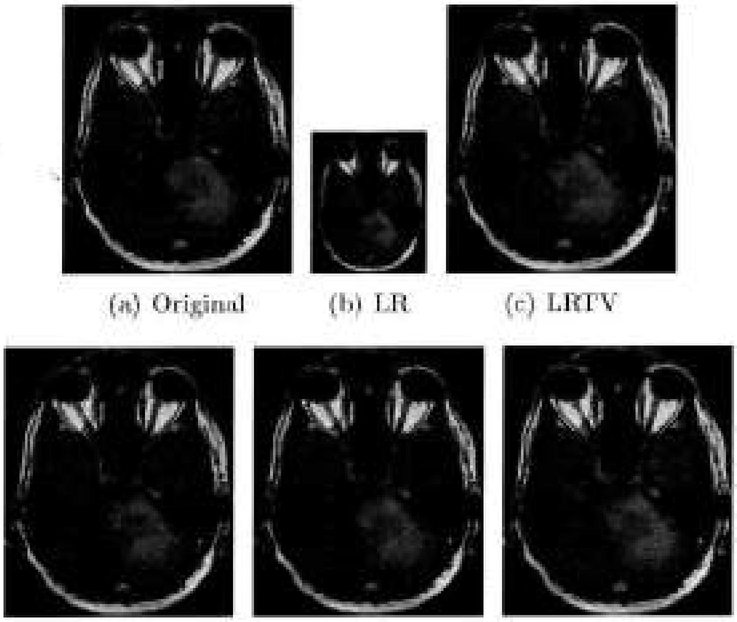

(a) Original (b) LR (c) LRTV

(d) ScSR (e) JRSR (f) Proposed

Figure 3.4: Comparison of reconstructed MRS images by different methods for upscale ratio 2

Table 3.1: Quantitative parameters resulted by different methods from two MRS test images using zooming value 2 and 3, respectively

	MRSI1 (Zoom = 2)				MRSI2 (Zoom = 3)			
Methods	PSNR	SSIM	FSIM	MI	PSNR	SSIM	FSIM	MI
LRTV[35]	31.34	0.9238	0.9209	3.080	29.69	0.8806	0.9077	1.989
ScSR[43]	36.57	0.9833	0.9821	4.012	35.01	0.9232	0.9643	2.563
JRSR[20]	39.20	0.9844	0.9854	**4.327**	35.36	0.9350	0.9837	**2.634**
Proposed	**40.82**	**0.9889**	**0.9881**	4.289	**35.78**	**0.9367**	**0.9854**	2.630

0.4 dB for 3x zooming for the two test images, respectively. In case of DW images, quite similar improvements are also observed in terms of PSNR for the proposed method than the SCSR. However, for the DW test images, the proposed method not only outperforms the JRSR, but corresponding improvements are even better as compared to those for the MRS test images. This may be probably due to the fact that the proposed sparse reconstruction method is applied only on the texture layers, which have significant high-frequency features. Similar observations are also made in case of the proposed method in terms of MSSIM and other parameters, when compared to others. From Figs. 3.4-3.11, it is clearly seen that the fine details such as edges and textures have been preserved better in case of the proposed method. The magnified views of a specified portion of the visual results show that fine details have been recovered well by the proposed method.

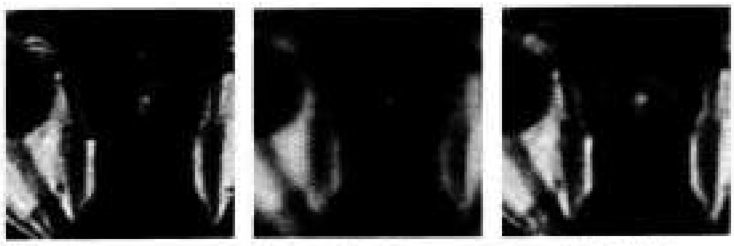

(a) Original (b) LR (c) LRTV

(d) ScSR (e) JRSR (f) Proposed

Figure 3.5: Comparison of magnified view of resulted MRS images by different methods for upscale ratio 2

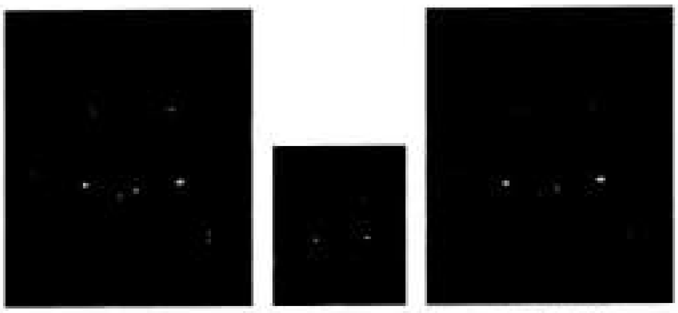

(a) Original (b) LR (c) LRTV

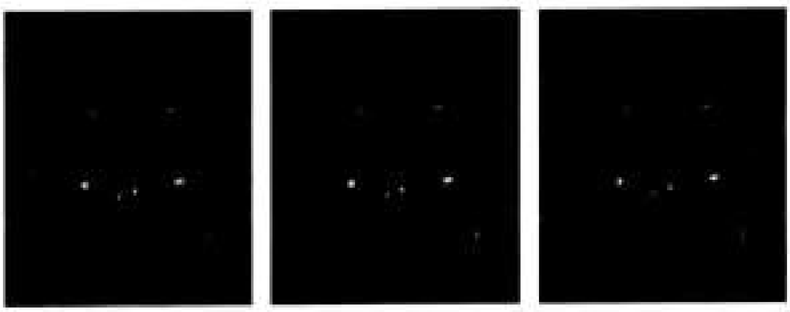

(d) ScSR (e) JRSR (f) Proposed

Figure 3.6: Comparison of reconstructed MRS images by different methods for upscale ratio 3

Table 3.2: Quantitative parameters resulted by different methods from two DW test images using zooming value 2 and 3, respectively

	DW1 (Zoom = 2)				DW2 (Zoom = 3)			
Methods	PSNR	SSIM	FSIM	MI	PSNR	SSIM	FSIM	MI
LRTV[33]	40.07	0.9851	0.9878	3.980	32.04	0.9215	0.9322	3.330
ScSR[43]	41.02	0.9880	0.9873	4.035	32.84	0.9301	0.9416	3.420
JRSR[30]	40.56	0.9879	0.9898	**4.298**	32.20	0.9281	0.9445	3.390
Proposed	**43.04**	**0.9915**	**0.9910**	4.233	**33.50**	**0.9388**	**0.9457**	**3.472**

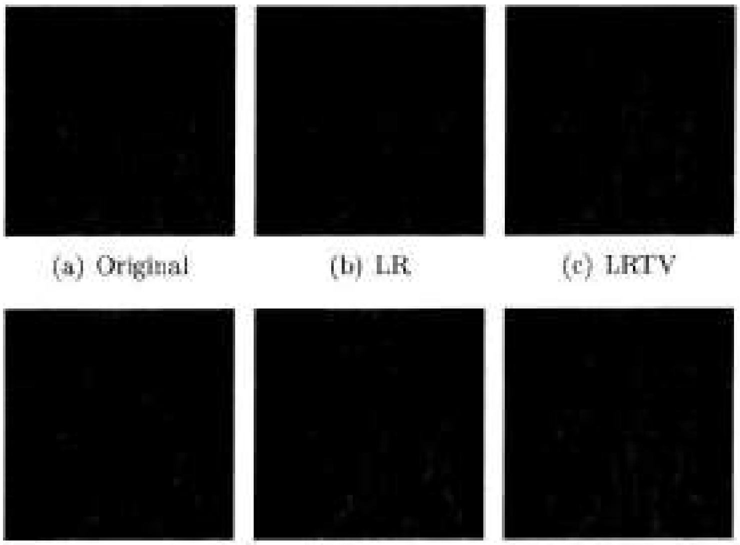

(a) Original (b) LR (c) LRTV

(d) ScSR (e) JRSR (f) Proposed

Figure 3.7: Comparison of magnified view of resulted MRS images by different methods for upscale ratio 3

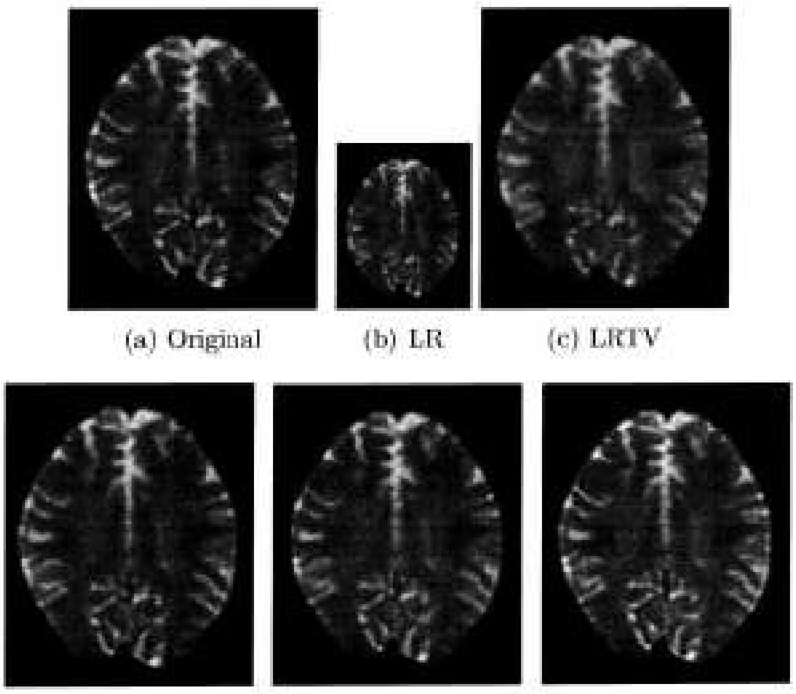

(a) Original (b) LR (c) LRTV

(d) ScSR (e) JRSR (f) Proposed

Figure 3.8: Comparison of reconstructed images for DW first test image by different methods and upscale ratio 2

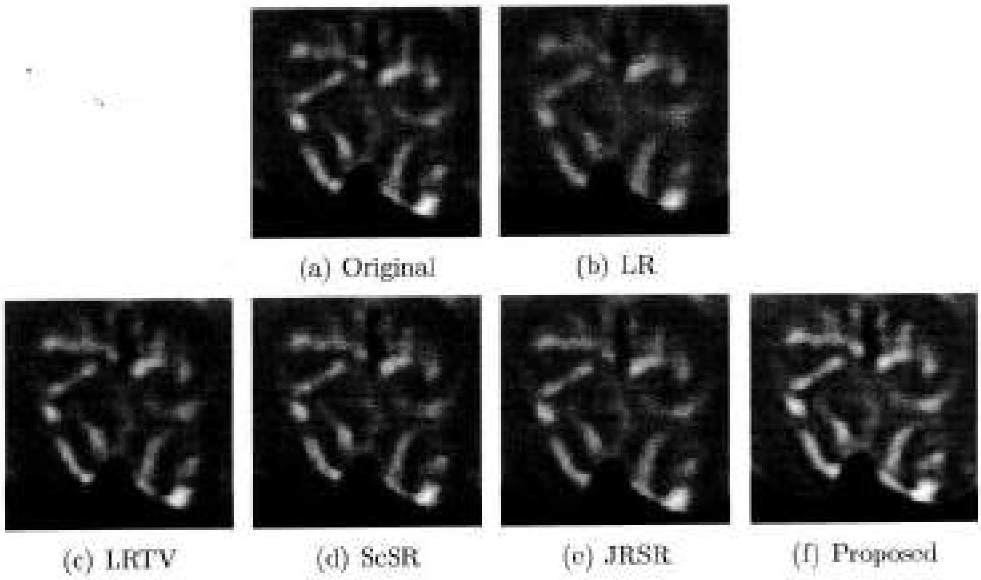

(a) Original (b) LR

(c) LRTV (d) ScSR (e) JRSR (f) Proposed

Figure 3.9: Magnified view comparison for DW first test image results by different methods and upscale ratio 2

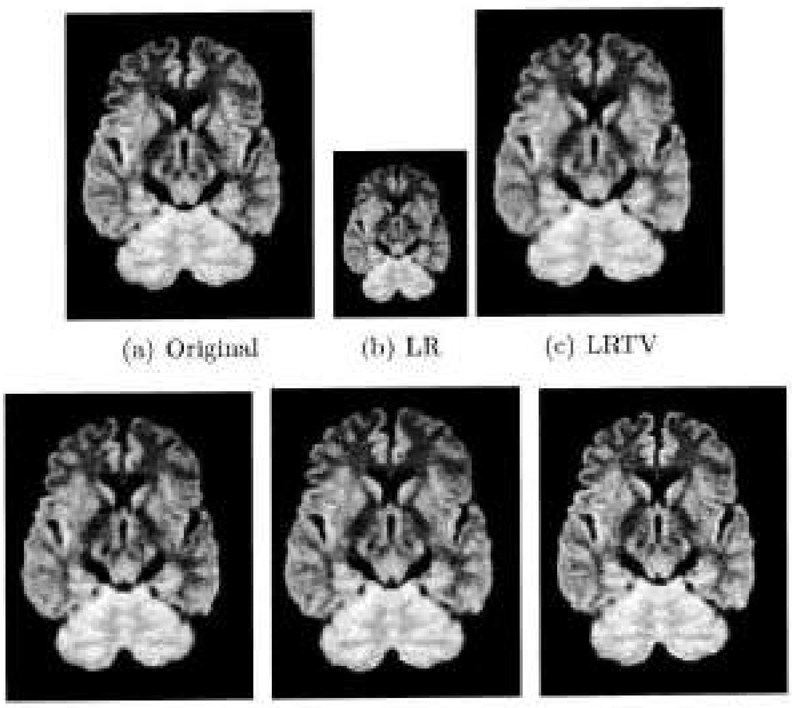

(a) Original (b) LR (c) LRTV

(d) ScSR (e) JRSR (f) Proposed

Figure 3.10: Comparison of reconstructed images for DW second test image by different methods and upscale ratio 3

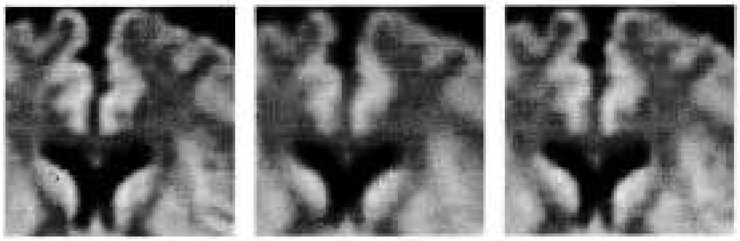

(a) Original (b) LR (c) LRTV

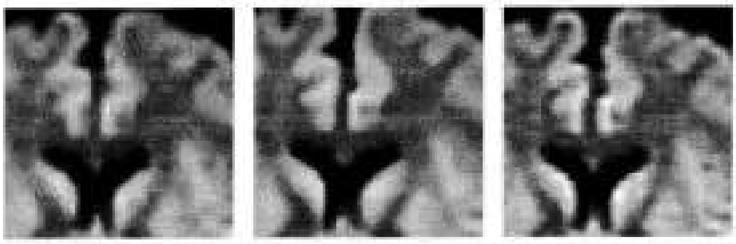

(d) ScSR (e) JRSR (f) Proposed

Figure 3.11: Magnified view comparison for DW second test image results by different methods and upscale ratio 3

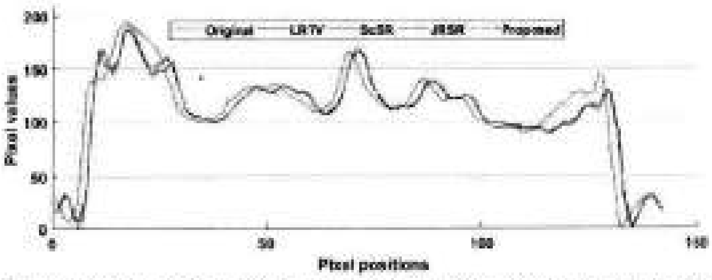

Figure 3.12: Comparison of central row profiles for reconstructed DW images with upscale ratio 2

Fig. 3.12 shows the central row profile comparison of result images produced by different SR methods. It is a plot of pixel values across a line in the image that is the central horizontal line, and it is used to compare the pixel-wise accuracy of the different reconstruction techniques. It can be observed that the proposed method gives the most closest profile to that of the original image's profile.

3.5 Conclusions

This chapter demonstrates that the SISR algorithm based on the sparsity over learned overcomplete dictionary along with a non-local TV regularization provides consistent SR outputs for clinical DW and MRS images at different upscale ratios. Simulation results prove that the proposed method is able to outperform other existing regularization based SR methods both in terms of visual and quantitative results. In terms of computational time, the proposed method is somewhat expensive due to the iterative process in the regularization techniques. Multicore parallel processing or general purpose graphics processing units (GP-GPUs) may be an alternative choice for the efficient implementation of this method to achieve clinically feasible performance. Research works are already in progress in this direction for real-time implementations.

CHAPTER 4

Diffusion-weighted and Spectroscopic MRI Super-resolution using Sparse Representations

In this chapter, we adopt a similar model as in Eq.(1.2) with an additional regularization term based on NLR for the SR of DW and MRS images. The proposed a novel sparse representation model based on sparsity priors using external HR datasets as well as non-local self-similarity of LR input to enhance spatial resolution of DW and MRS images and implemented the proposed algorithm in a general purpose graphics processing unit (GP-GPU) and CPU environment to achieve clinical relevance. The proposed method carries out SR is discussed in the following sections. It consist of four main stages: *Dictionary Training*, *Feature Extraction*, *Joint Sparse Coding* and the *SR Reconstruction*.

4.1 Dictionary Training

Two overcomplete dictionaries (low ($\mathbf{T}_\ell$) - and high-resolution ($\mathbf{T}_h$), respectively) are to be invoked during the training process; one supposed to represent the low resolution patches and the other high resolution patches. Training is carried out using an external image dataset of already available good quality MR images, which may be assumed as available HR images not related to test images. Dictionaries are to be learnt jointly in order to preserve compatibility of HR patches to be generated during the iterative patch reconstruction process with their neighbors. During the training, a joint sparse representation problem is solved iteratively involving a joint or coupled overcomplete dictionary, $\mathbf{T}_c = (\mathbf{T}_\ell; \mathbf{T}_h)$, which yields a single sparse coding vector assuming that low- and high-resolution patches share a unique representation. After every iteration, the atoms of the joint dictionary are updated with the current sparse solution. A schematic representation of the dictionary training process using sparse representation is shown in Fig. 4.1.

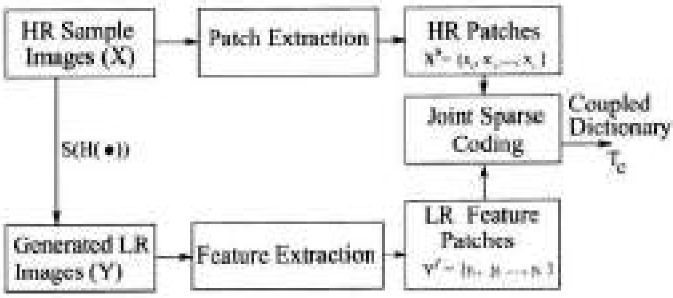

Figure 4.1: Coupled dictionary training

We extract both HR and LR patch vectors, $\mathbf{x}$ and $\mathbf{y}$, respectively from the HR training dataset. Note that patch vectors $\mathbf{x}$ are extracted directly from the HR training dataset while the feature patch vectors $\mathbf{y}$ are extracted from the blurred and downsampled version of sample HR images.

4.1.1 Feature Extraction

Since LR image patches are used for sparse representation, it is important to make them more favorable candidates for sparse representation by removing redundant low-frequency information present in them. To achieve this, the LR image is passed through a feature extraction step that provides the available high-frequency information in it. As reported by Yang *et al.* [43], we extract gradient features by applying four 1-D derivative filters of orders 1 and 2, for finding the horizontal and vertical features, e.g. edges, contours, etc.

We obtain four gradient maps after applying these 1D filters separately on each LR image. Now, corresponding to each feature position, we obtain four feature patches, one from each gradient map, and finally concatenate them as a single vector after vectorizing each patches. This yields LR feature vectors: Y^{ℓ} which is given as $Y^{\ell} = \{\mathbf{y}_1, \mathbf{y}_2, \ldots, \mathbf{y}_k\}$ corresponding to k HR patch vectors: $X^h = \{\mathbf{x}_1, \mathbf{x}_2, \ldots, \mathbf{x}_k\}$.

In this process of feature extraction for LR patches also bears information of its neighborhood, essential for accurate HR image reconstruction.

4.1.2 Joint Sparse Coding

Low- and high-resolution dictionaries: $\mathbf{T}_\ell$ and $\mathbf{T}_h$ are jointly trained so that sparse coding vector for HR and LR patches is the same. We concatenate HR patch vectors, X^h and LR feature vectors, Y^ℓ into a single vector X_c. Then a sparse representation problem is formulated using the joint dictionary $\mathbf{T}_c$ and X_c for dictionary learning. Mathematically,

$$\min_{\{\mathbf{T}_c, A\}} ||X_c - \mathbf{T}_c A||_2^2 + \lambda(\frac{1}{p'} + \frac{1}{q'})||A||_1, \tag{4.1}$$

where $X_c = \begin{bmatrix} \frac{1}{\sqrt{p'}} X^h \\ \frac{1}{\sqrt{q'}} Y^\ell \end{bmatrix}$, $\mathbf{T}_c = \begin{bmatrix} \frac{1}{\sqrt{q'}} \mathbf{T}_h \\ \frac{1}{\sqrt{p'}} \mathbf{T}_l \end{bmatrix}$, and columns of A contain sparse coefficient vectors of corresponding image patches, i.e. $A = \{\alpha_1, \alpha_2, \ldots, \alpha_k\}$. Here, p' and q' are the lengths of $\mathbf{x}$ and $\mathbf{y}$, respectively. Eq. 4.1 is the standard basis pursuit problem, which is efficiently solved using the feature-sign search based approach [25].

4.2 SR Image Reconstruction

The proposed SISR model modifies Eq. 1.2 to include both the external and internal a priori information as its regularizing terms during the iterative reconstruction of the desired SR output from a given LR MR image. Thus, a new model may be defined as follows:

$$\hat{\mathbf{X}} = \arg\min_{\mathbf{X}} ||SH\mathbf{X} - \mathbf{Y}||_2^2 + \lambda_1 \Psi_{\text{sparsity}}(\mathbf{X}) + \lambda_2 \Psi_{\text{NLR}}(\mathbf{X}), \tag{4.2}$$

where λ_1 and λ_2 are two regularization parameters and the second term is to impose sparsity of the input image over an image transform or a learned overcomplete patches in an iterative manner such that the reconstrcuted HR patches maintain a close similarity with their neighbors, which may be reproduced here as follows:

$$\Psi_{\text{sparsity}}(\mathbf{X}) = \sum_i \tfrac{1}{2} \left\| \tilde{\mathbf{y}}_i - \tilde{\mathbf{T}} \boldsymbol{\alpha}_i \right\|_2^2 + \lambda \left\| \boldsymbol{\alpha}_i \right\|_1, \tag{4.3}$$

where $\tilde{\mathbf{T}} = \begin{pmatrix} R\,\mathbf{T}_l \\ P\,\mathbf{T}_h \end{pmatrix}$, $\tilde{\mathbf{y}}_i = \begin{pmatrix} \mathbf{y}_i \\ \beta\,\mathbf{w} \end{pmatrix}$, $\mathbf{y}_i = R\ (SH\mathbf{X})$ is the i^{th} LR feature patch extracted using operator R and $\mathbf{w}$ represents pixel values from the previously reconstructed HR image on the overlap, extracted using operator P. Similarly, the third term in Eq. 4.2 is another regularization term that exploits the non-local self-similarity through non-local rank minimization and defined as follows:

$$\Psi_{\text{NLR}}(\mathbf{X}) = \sum_j \tfrac{1}{2} \left\| \Gamma_j \mathbf{X} - \mathbf{L}_j \right\|_2^2 + \gamma \operatorname{Rank}(\mathbf{L}_j), \tag{4.4}$$

where Γ_j is a patch extraction operator that extracts patches for the j^{th} search window from $\mathbf{X}$.

Eq. 4.2 is a composite regularization problem and may be solved by using the concept of variable splitting technique [12, Chapter 3]. The main problem is split into three simpler sub-problems with respect to variables $\boldsymbol{\alpha}$, $\mathbf{L}$ and $\mathbf{X}$, respectively. We now define them as follows:

$$\hat{\boldsymbol{\alpha}} = \arg\min_{\boldsymbol{\alpha}} \sum_i \left(\tfrac{1}{2} \left\| \tilde{\mathbf{y}}_i - \tilde{\mathbf{T}} \boldsymbol{\alpha}_i \right\|_2^2 \right) + \beta \left\| \boldsymbol{\alpha}_i \right\|_1, \tag{4.5a}$$

$$\hat{\mathbf{L}} = \arg\min_{\mathbf{L}} \textstyle\sum_j \left(\tfrac{1}{2} \left\| \Gamma_j \mathbf{X} - \mathbf{L}_j \right\|_2^2 + \gamma \operatorname{Rank}(\mathbf{L}_j) \right), \tag{4.5b}$$

$$\begin{aligned} \hat{\mathbf{X}} = \arg\min_{\mathbf{X}} \tfrac{1}{2} \left\| SH(\mathbf{X}) - \mathbf{Y} \right\|_2^2 &+ \lambda_1 \sum_i \left(\tfrac{1}{2} \left\| R\ (SH(\mathbf{X})) - R\ \mathbf{T}_\ell \boldsymbol{\alpha}_i \right\|_2^2 \right) \\ &+ \lambda_2 \sum_j \left(\tfrac{1}{2} \left\| \Gamma_j \mathbf{X} - \mathbf{L}_j \right\|_2^2 \right), \end{aligned} \tag{4.5c}$$

where R is the patch extraction operator. First subproblem is solved by the feature-sign search algorithm as done by [13, 43]. Next subproblem is a low-rank minimization problem and can be solved efficiently using the singular value decomposition [illegible] their results are inserted in the third subproblem. This leaves the third subproblem into a form of simple least-square minimization problem, whose close form solution can be obtained by differentiating it w.r.t. $\mathbf{X}$. We term it as the Sparse Representation and non-local low-rank regularization (SRNLR) algorithm. Algorithmic steps of SRNLR are summarized in Algorithm 2. The initial HR image $\mathbf{X}^0$ is obtained

Algorithm 2 SRNLR Reconstruction algorithm

Input: $\mathbf{Y}$, S, H, R, Γ, $\tilde{\mathbf{T}}$
Initialization: $k \leftarrow 0$, $\varepsilon \leftarrow 10^{-4}$, $\mathbf{X}^0$, β, γ, λ_1, λ_2
while not converge **do**
  $k \leftarrow k+1$
  $\boldsymbol{\alpha}^k \leftarrow \arg\min\limits_{\boldsymbol{\alpha}} \sum\limits_i \left(\frac{1}{2} \left\| R(SH(\mathbf{X})) - \tilde{\mathbf{T}}\boldsymbol{\alpha}_i \right\|_2^2 \right) + \beta \left\| \boldsymbol{\alpha}_i \right\|_1$
  $\mathbf{L}^k \leftarrow \arg\min\limits_{\mathbf{L}} \sum\limits_j \left(\frac{1}{2} \left\| \Gamma_j \mathbf{X} - \mathbf{L}_j \right\|_2^2 + \gamma \, \mathrm{Rank}(\mathbf{L}_j) \right)$
  $\mathbf{X}^k \leftarrow \frac{(SH)^t \mathbf{Y} + \lambda_1 \sum_i (RSH)^t R \mathbf{T}_i \boldsymbol{\alpha}_i + \lambda_2 \sum_j \Gamma_j^t L_j}{(SH)^t SH + \lambda_1 \sum_i (RSH)^t RSH + \lambda_2 \sum_j \Gamma_j^t \Gamma_j}$
  check convergence : $\left\| \mathbf{X}^k - \mathbf{X}^{k-1} \right\| / \left\| \mathbf{X}^k \right\| \leqslant \varepsilon$
end while
Output: $\mathbf{X}^* \leftarrow \mathbf{X}^k$

using bicubic interpolation of the LR input image $\mathbf{Y}$.

4.3 Results And Discussion

4.3.1 Database Preparation

Databases of DW and MRS images are acquired from MRI scanners installed in two local Hospitals, namely, Apollo Hospitals, Guwahati and GNRC, Guwahati Six mile. DW images are acquired using scanners- GE 1.5 T SIGNA Explorer with following parameter settings: scanning sequence: GR, matrix size: 256×256, TR/TE: 47.5 msec./ 2.6 msec., slice thickness: 5 mm, no. of averages: 1, and GE 1.5 T SIGNA HDxt with scanning sequence: EP/SE, matrix size: 256×256, TR/TE: 4225 msec./ 77.9 msec., slice thickness: 5 mm, no. of averages: 2. On the other hand MRS images are acquired using a GE 1.5 T SIGNA Explorer with following parameter settings: scanning sequence: EP/SE, matrix size: 256×256, TR/TE: 4313 msec./ 85.2 msec., slice thickness: 5 mm, no. of averages: 1.

Dictionaries are trained for DW and MRS images separately. In each case, training is done using 30-40, 256×256 brain images of axial, coronal, and sagittal cross sections. These images are selected such that they contain significant features, like edges, textures in them. Training is to be performed using prototype signals, which are extracted as overlapping patches from the selected datasets. A few sample images for training are shown in Fig. 4.2. We produce corresponding LR versions of training images in our simulations by applying blurring and down-sampling operations on high quality images. In order to display the performance of SR reconstruction of the proposed method, a pair of test images, Test 1 and Test 2 are shown in Fig. 4.3 from each of the DW and MRS datasets, respectively which are representatives of our several other test images.

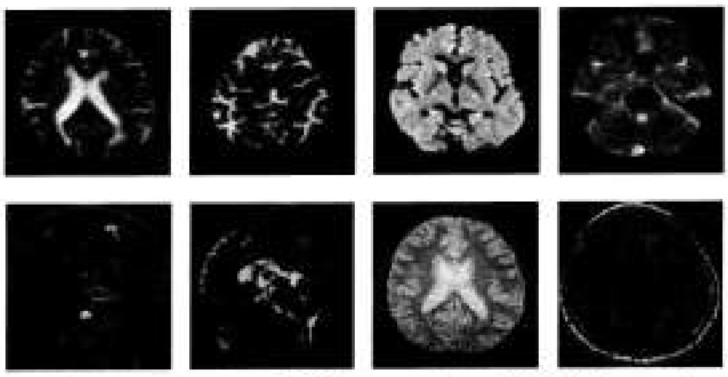

Figure 4.2: Training images: DW (top row) and MRS image (bottom row)

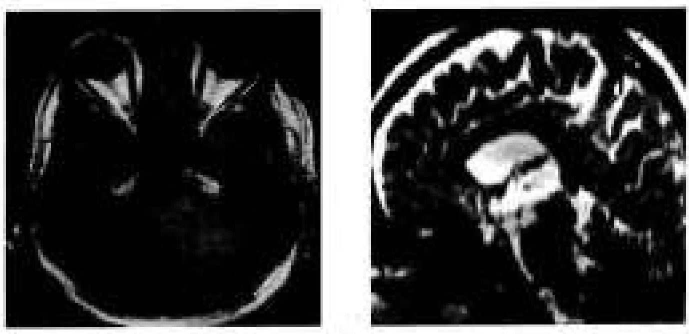

(a) Test1 (b) Test2

Figure 4.3: Test images: MRS (left) and DW (right) images

4.3.2 Simulation Environment

Simulations are carried out in MATLAB environment on a workstation having specifications as follows: Intel(R) Xeon(R) CPU E5-2650 v4 @ 2.20 GHz, 2201 MHz and 12 Cores; GPGPU: NVIDIA Quadro P5000 with 16 GB GDDR5X memory and 2560 CUDA cores.

4.3.3 Simulation Results

In this work, experiments are conducted to perform SR of DW and MRS images by different upscale ratios. LR images are first obtained by downsampling selected high quality MR images by a factor equal to the upscale ratio. The blurring in the generated LR image is done by applying a Gaussian low-pass filter (LPF) with kernel size 5 and $\sigma = 1.5$ for downsampling by $\frac{1}{2}$. Similarly, for downsampling by $\frac{1}{4}$ these parameters are fixed at 7 and 1.6, respectively. We neglect the additive noise term in Eq. 1.1 while producing the LR MR image as the SR reconstruction by sparse regularization technique implicitly removes any additive noise during the iterative reconstruction process. Now, for joint dictionary learning, we extract over 1,00,000 LR/HR patch pairs from each of the training datasets separately, i.e. DW and MRS, considering a patch size of 5×5 with two pixels overlap between two adjacent patches. To test the reconstruction performances, dictionaries of different number of atoms, e.g. 256, 512, 1024 and 2048 are trained. It is observed that computational time for dictionary learning increases drastically as number of atoms increases beyond 512 with no significant improvements in terms of SR reconstruction. Therefore, we conduct our experiments with a fixed dictionary size of 512 for optimal performance.

Five parameters have been used for quantitative evaluations of the reconstructed images with reference to the ground truth. Besides the commonly used evaluation metrics like, signal-to-noise ratio (SNR) and mean structural similarity index (MSSIM), a few other MR image evaluation parameters are also considered for fair comparisons. They are as follows: mutual information (MI) [7]: it is a measure of the degree of statistical dependence between two random variables; feature similarity index measure (FSIM) [51]: it is based on measuring phase congruency (PC) and gradient magnitude (GM) while characterizing local image quality, and gradient magnitude similarity deviation (GMSD) [41]: it is based on exploring global variation of gradient based local quality map for overall image quality prediction. For a better SR reconstruction, the values of SNR, MSSIM, MI, FSIM should be high, and GMSD should be small. As in real-world applications or in clinical practice, there will be no ground truth as such, so in addition to the reference based metrics, we apply a no-reference based metric for evaluation of SR outputs without any bias. A widely used no-reference parameter for evaluation of SR reconstruction is the natural image quality evaluator (NIQE) [17], which measures image quality by calculating the input image's local statistics. A smaller NIQE value indicates a better image quality.

To compare the performance of the proposed algorithm with state-of-the-art methods, we have considered six different methods including two most recent algorithms, namely, the CRNS [11] and the JRSR [10], reported in 2018.

MRS Image SR

SR reconstructions for Test 1 are shown in Figs. 4.4-4.5 for upscale ratios of 2 and 4, respectively. For visual comparisons of reconstructed images, a small portion of the SR output is also selected and zoomed in for better identifications of the details. It can be observed that the proposed method gives better visual representation of the reconstructed image with enhanced edge information compared to the state-of-the-art. Besides visual analysis, validation of the results are also done with different objective measures, which are used in the SR literature and shown in Table 4.1. It can be observed that the proposed method outperforms other methods in terms of all the parameters. An average improvement of about 3.27 dB and 1.14 dB in SNR are achieved by the proposed method over the CRNS method for 2 and 4 times upscaling, respectively. Similarly, an improvement of 3 dB and 0.73 dB in SNR are achieved, respectively compared to the JRSR. It can be observed that the JRSR performs better than the CRNS for higher zooming factors. Significant improvements are also observed in terms of MSSIM and other parameters in case of the proposed method. We infer that in case of MRS image SR, the proposed method is proved to be much more effective than recent SR methods.

DW Image SR

Visuals of reconstructed images by different algorithms for the Test 2 image are presented in Figs. 4.6- 4.7 for upscale ratios of 2 and 4, respectively. We observe that the proposed method gives the best representation of details in the reconstructed images than its counterparts. It is seen that bicubic introduces significant blurring in the output image, similar is the case for EDI. In comparison to the JRSR and CRNS, the proposed method provides less smoothing and better preservation of edges. Next, quantitative evaluations are also carried out for all the methods using the same parameters as discussed above. As shown in Table 4.2, for the proposed method, on an average SNR is 0.92 dB more compared to the CRNS for an upscale ratio of 2, while the it is 1.74 dB more in case of upscale ratio of 4. However, JRSR is found to work better than CRNS in case higher zooming factors. We observe an average improvement of 0.71 dB in case of the proposed method than the JRSR for an upscaling by 4. Improvements are also observed in case of the proposed method in terms of other quantitative parameters- MSSIM, FSIM, etc. This conforms to our findings during the visual analysis.

Table 4.3 shows NIQE values using different zooming factors for state-of-the-art methods. It is observed that outputs of the proposed method are more closer to the original in terms of NIQE, which clearly states the proposed method is able to restore fine details and other structures better than CRNS and JRSR. Similar is the observation for the proposed method when compared to ScSR except at 4 times upscaling of MRS image. For higher zooming factors, NIQE also increases, indicating that reconstruction quality degrades with the increase in upscaling factors, which is natural.

From the analysis of results for MRS and DW images as discussed above, we conclude that the proposed method proves to be very efficient in preserving sharp edges and structural details. This is the major objective of any SR method as human eyes are more sensitive to these details, which is being fulfilled by the proposed method very effectively. This is further corroborated by corresponding error images shown in Fig 4.8.

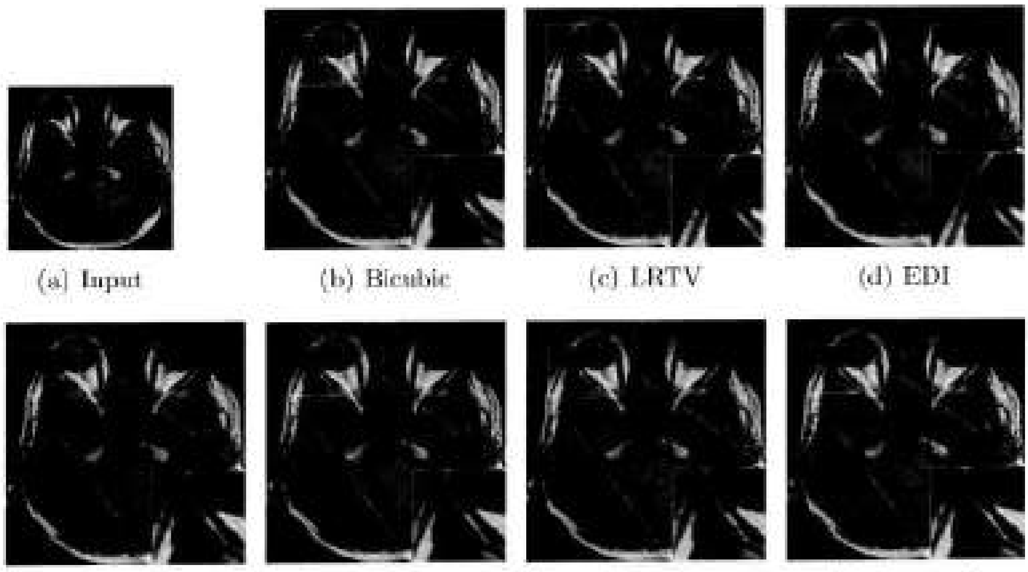

(a) Input (b) Bicubic (c) LRTV (d) EDI

(e) ScSR (f) CRNS (g) JRSR (h) Proposed

Figure 4.4: SR results of Test 1 by using different techniques for upscale factor 2

k-fold Validation

Experiments are conducted using a database of 25 images for 5-fold cross-validation in order to remove any bias of the learned dictionary model towards a particular dataset during reconstruction. LR images of a given fold is upscaled using the proposed method where the required dictionary is trained using the HR images of the remaining folds. In this manner, the experiment is repeated 5 times by considering different groups containing 5 test and 20 training images. Validation has been done by computing different quantitative evaluation metrics for the resulted images for all the test images. An average of five different values obtained from the five folds of a quantitative evaluation metric is considered as the best possible value of that metric and reported in Table 4.4 for different methods. Results show the superiority of the proposed method.

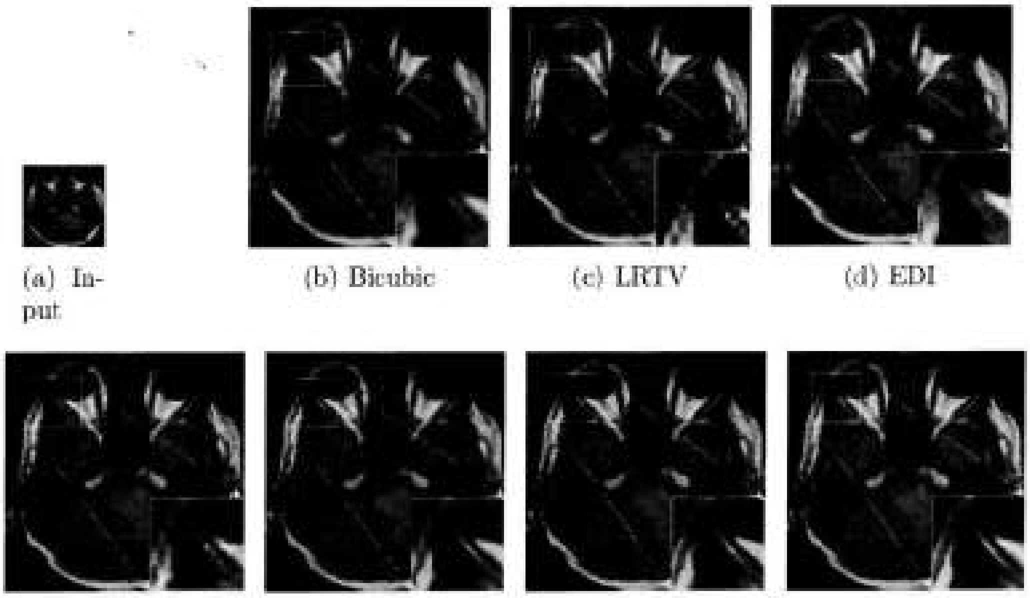

(a) Input (b) Bicubic (c) LRTV (d) EDI

(e) ScSR (f) CRNS (g) JRSR (h) Proposed

Figure 4.5: SR results of Test 1 by using different techniques for upscale factor 4

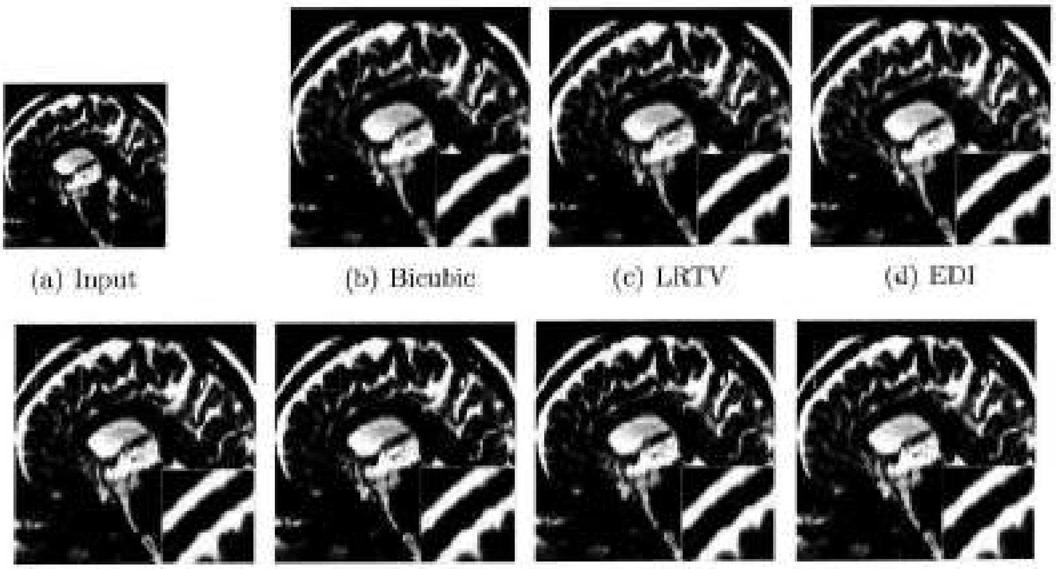

(a) Input (b) Bicubic (c) LRTV (d) EDI

(e) ScSR (f) CRNS (g) JRSR (h) Proposed

Figure 4.6: SR results of Test 2 by using different techniques for upscale factor 2

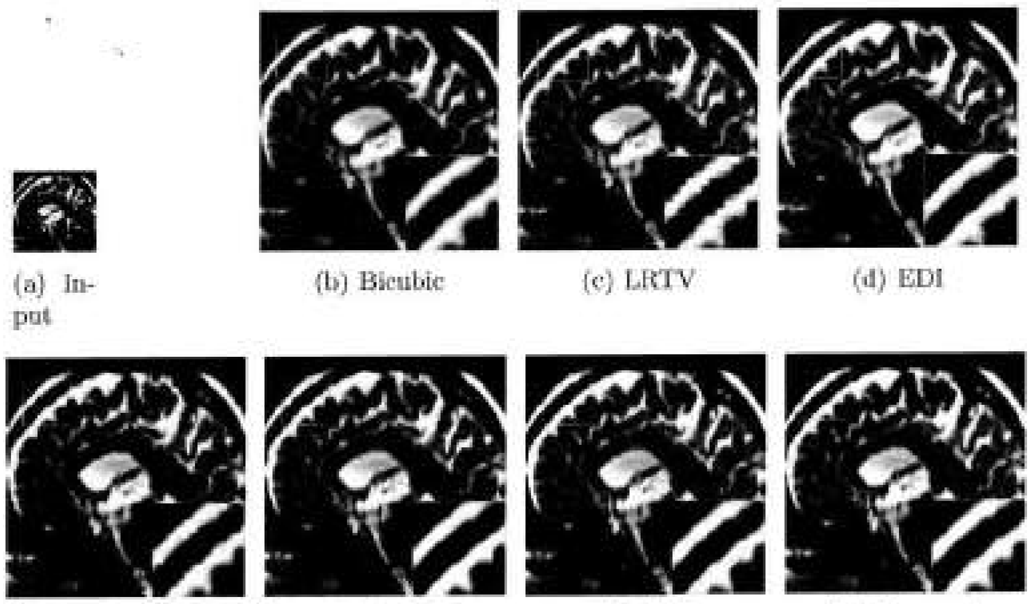

(a) Input (b) Bicubic (c) LRTV (d) EDI

(e) ScSR (f) CRNS (g) JRSR (h) Proposed

Figure 4.7: SR results of Test 2 by using different techniques for upscale factor 4

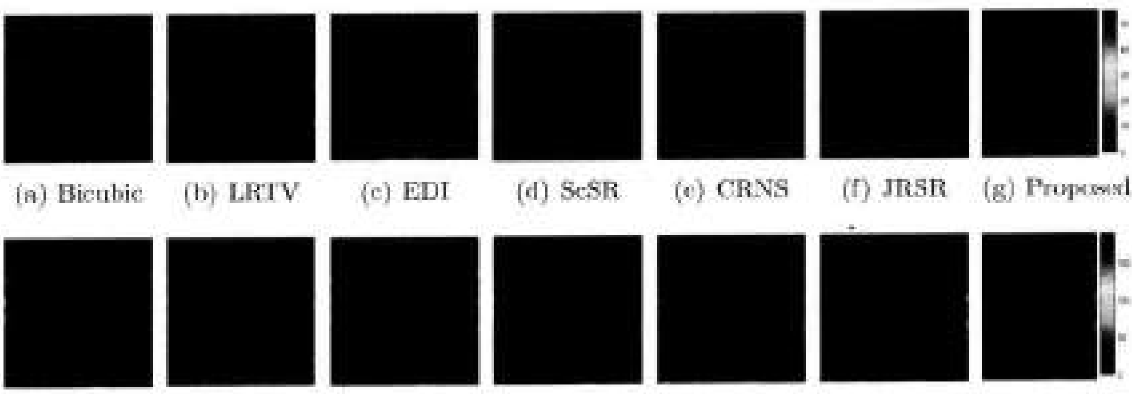

(a) Bicubic (b) LRTV (c) EDI (d) ScSR (e) CRNS (f) JRSR (g) Proposed

(h) Bicubic (i) LRTV (j) EDI (k) ScSR (l) CRNS (m) JRSR (n) Proposed

Figure 4.8: Error images between original and reconstructed images: first row (a-g) shows results for Test 1 by 2 times; second row (h-n) shows the results for Test 2 by 4 times.

4.3.4 Comparison of Computational Time

Computational time (in seconds) required for sequential implementation of different SISR methods for zooming factors of 2 and 4 are shown graphically in Fig. 4.10. In this case, the target HR image is of size 256×256 and the input LR images are of size 128×128 and 64×64, respectively. We observe that sequential implementation of the proposed method takes more time compared to the JRSR but less than the CRNS. In order to improve the computational time, we also implement the proposed algorithm using CUDA Mex in MATLAB and GP-GPU, which will be discussed later.

4.3.5 Simulations with Synthetic Image

In order to get an idea of the performance of the proposed method for real-world applications without HR ground-truth images, we consider a synthetic image available in MATLAB. Overcomplete dictionaries are learnt from a dataset of phantom images taken from the internet. For reconstruction, we consider 128×128 synthetic image as LR image then its SR outputs are obtained using the proposed method for zooming factors 2, 4, and 8. Synthetic images of dimensions equal to those of SR outputs as described above are also generated using the MATLAB program for visual comparisons. Fig. 4.9 shows SR outputs for different zooming factors along with corresponding values of SNR. Results indicate that the proposed method is able to zoom the synthetic image for any dimension and still maintain the structural conformity with their LR counterparts and could preserve sharp edges accurately.

4.3.6 Parallel Implementation in CPU-GPU Environment

Sequential execution of the proposed algorithm consumes large time as it requires to solve two subproblems iteratively, namely, sparse optimization and the non-local similarity based regularizations, iteratively. Moreover, these subproblems are solved patch wise. Further, clinical DW and MRS images contain a number of slices, which further blows up the dimensionality of the SR problem. Hence, sequential implementation of the proposed algorithm will not be applicable in real medical applications. Therefore, in this work, an implementation framework using both CPU and general purpose graphics processing unit (GPGPU) is utilized to speed up the overall algorithm. Computationally expensive operations, like patch-wise

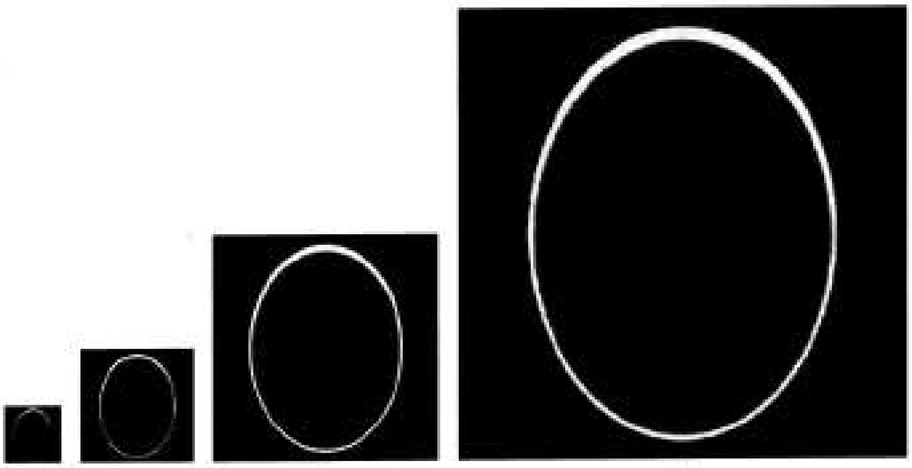

(a) (b) (c) (d)

Figure 4.9: Visual results with a synthetic image using the proposed method: (a) input 128×128 (b) upscale 2 (256×256), SNR value: 17.39 dB (c) upscale 4 (512×512), SNR value: 16.72 dB and (d) upscale 8 (1024 × 1024), SNR value: 13.54 dB

Table 4.1: Reference based performance evaluation for Test 1

Upscale	Parameters	Bicubic	LRTV	EDI	ScSR	CRNS	JRSR	Proposed
2	**SNR (dB)**	23.24	25.60	23.60	27.38	26.93	27.20	**30.20**
	MSSIM	0.9530	0.9740	0.9470	0.9735	0.9808	0.9738	**0.9879**
	GMSD	0.0255	0.0036	0.0178	**0.0014**	0.0028	0.0034	0.0020
	MI	3.387	3.073	3.280	3.794	4.104	3.724	**4.188**
	FSIM	0.9803	0.9697	0.9185	0.9777	0.9847	0.9715	**0.9875**
4	**SNR (dB)**	15.38	16.89	15.43	16.96	17.37	17.78	**18.51**
	MSSIM	0.7998	0.8060	0.6972	0.8277	0.8479	0.8530	**0.8608**
	GMSD	0.1127	0.1016	0.1322	0.0932	0.0886	0.0823	**0.0756**
	MI	2.117	2.491	2.279	2.524	2.694	2.719	**2.725**
	FSIM	0.8382	0.8361	0.7041	0.8618	0.8778	0.8700	**0.8876**

Table 4.2: Reference based performance evaluation for Test 2

Upscale	Parameters	Bicubic	LRTV	EDI	ScSR	CRNS	JRSR	Proposed
2	**SNR (dB)**	26.91	27.30	26.47	28.58	30.93	30.10	**31.85**
	MSSIM	0.9765	0.9818	0.9696	0.9822	0.9872	0.9840	**0.9887**
	GMSD	0.0146	0.0128	0.0156	0.0048	0.0055	**0.0042**	0.0043
	MI	3.898	3.921	3.739	3.997	4.309	4.137	**4.359**
	FSIM	0.9736	0.9803	0.9695	0.9806	0.9891	0.9861	**0.9899**
4	**SNR (dB)**	18.71	18.48	17.34	19.87	19.93	20.96	**21.67**
	MSSIM	0.8585	0.8570	0.8126	0.8808	0.8994	0.9041	**0.9161**
	GMSD	0.0976	0.0907	0.1011	0.0807	0.0814	0.0703	**0.0656**
	MI	2.787	2.704	2.517	2.868	3.036	3.034	**3.131**
	FSIM	0.8549	0.8749	0.8745	0.9054	0.9223	0.9202	**0.9332**

operations within sparse optimization are implemented using CUDA mex and rest are implemented using C++ mex in MATLAB environment. Besides, we also use

Table 4.3: No-reference based performance evaluation on test images in terms of SNR (dB) for different upscale factors

Image	Upscale	ScSR	CRNS	JRSR	Proposed	Original
Test 1	2	19.52	22.29	22.95	18.30	17.15
	4	28.16	31.00	34.38	33.54	17.15
Test 2	2	26.50	26.55	26.51	24.61	23.77
	4	41.22	35.43	37.36	29.92	23.77

Table 4.4: k-fold validation for SR reconstruction

Parameters	MRSI			
	× 2		× 4	
	ScSR	Proposed	ScSR	Proposed
SNR (dB)	26.4303±3.402	27.7953±3.790	17.3336±2.862	18.4444±2.4219
SSIM	0.9804±0.0108	0.9849±0.0086	0.8395±0.0060	0.8739±0.0303
MI	4.2850±0.5525	4.5924±0.5931	2.7835±0.3636	3.0457±0.3326
FSIM	0.9751±0.0060	0.9803±0.0079	0.8590±0.0217	0.8829±0.0157
Parameters	**DW-MRI**			
	× 2		× 4	
	ScSR	Proposed	ScSR	Proposed
SNR (dB)	39.7584±2.181	43.1674±3.481	26.5060±5.826	30.3824±5.705
SSIM	0.9947±0.0011	0.9972±0.0013	0.9188±0.0618	0.9527±0.0593
MI	4.8766±0.4509	5.3486±0.4951	3.4029±0.7093	3.8625±0.8293
FSIM	0.9966±0.0019	0.9981±0.0008	0.9429±0.0413	0.9627±0.0249

Table 4.5: Comparison with a deep learning based approach in terms SNR and MSSIM

Image	Upscale factor	Method	SNR (dB)	MSSIM
MRS	2×	VDSR	25.06	0.9799
		Proposed	30.20	0.9879
	4×	VDSR	18.39	0.8062
		Proposed	18.51	0.8608
DW	2×	VDSR	27.03	0.9711
		Proposed	31.85	0.9887
	4×	VDSR	18.99	0.8513
		Proposed	21.07	0.9161

Table 4.6: Sequential and parallel implementation time for SR of multi-slice MRI

Data	Upscale Factor	Input Size	Output Size	Sequential Time (secs.)	Parallel Time (secs.)
3D Spectroscopic MRI	2	128 × 128 × 24	256 × 256 × 24	8491	592.59
	4	64 × 64 × 24	256 × 256 × 24	14548	573.57
3D DW-MRI	2	128 × 128 × 25	256 × 256 × 25	11542	712.38
	4	64 × 64 × 25	256 × 256 × 25	15833	865.72

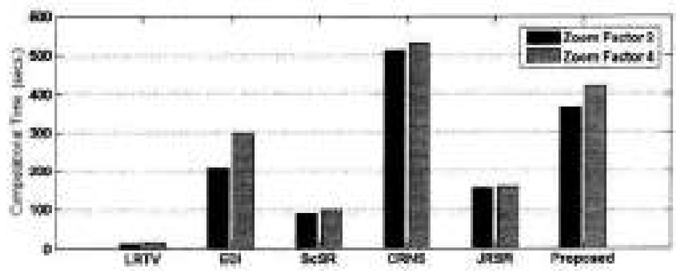

Figure 4.10: Comparison of Computational Time

parallel pool from MATLAB parallel computing toolbox for multi-core execution for a complete MRI dataset. Comparisons of computational times for both sequential and parallel implementations using clinical DW and MRS images are shown in Table 4.6. On an average, a speed-up (sequential to parallel time ratio) of about 16-20 times is achieved by the proposed CPU-GPGPU based parallel implementation.

4.3.7 Comparison with Deep Learning based Approach

For comparison with the deep learning-based approach, we have considered one of the well known deep learning-based SISR methods, namely, the super-resolution using very deep convolutional networks (VDSR) [24]. The VDSR network consists of 20-layers, and it takes 5 to 7 hours for training, whereas methods, like the SRCNN [14] consists of 3 layers and takes several days for training. One more key advantage of VDSR is that one can train it for multi-scale modeling i.e., the same network works for multiple scale factors after training. Separate datasets of MRS and DW images, consisting of 33 and 45 images, respectively are used for training with networks parameter settings as done in [24]. A quantitative comparison with the proposed method using both test images for different scale factors are shown in Table 4.5. We can observe that the proposed method gives better performance in all cases, irrespective of the scale factor, and images.

4.4 Conclusions

We demonstrate a novel SISR method using sparse reconstruction based on image sparsity and non-local self similarity. Extraction of prior information both external and internal is proved to be very efficient in preserving detailed information in super-resolved clinical DW and MRS images. Visual and quantitative comparisons with state-of-the-art SR methods have demonstrated the superiority of the proposed method. It is validated both for real MR and synthetic images; found its potential of GP-GPU hardware to get computationally efficient results, makes the proposed algorithm not only highly effective but also practically doable.

CHAPTER 5

Conclusions and Future Research Work

Present project report investigates a development of parallel processing embedded hardware for super-resolution of diffusion weighted and spectroscopic magnetic resonance images.

Chapter 1 discusses the short introduction and the clinical relevance of diffusion-weighted imaging (DWI) and spectroscopic magnetic resonance imaging (MRSI). This chapter also presents related work on sparse representation based MR image super-resolution techniques. The limitations of DWI and MRSI is discussed along with challenges faced in this images.

In **Chapter 2**, we have shown that the implementation of non-local TV regularization for solving the regularization issues of the sparsity based approach can be a viable solution to the issues. This combination provides better consistency of patches, thereby giving better results. Quantitative comparisons show that the proposed method outperforms the existing regularization based approaches. Proposed method is computationally expensive due to the iterative process of regularization.

In **Chapter 3**, we aim to develop a sparse representation based SISR algorithm based on the sparsity over learned overcomplete dictionary along with a non-local TV regularization provides consistent SR outputs for clinical DW and MRS images at different upscale ratios. Simulation results prove that the proposed method is able to outperform other existing regularization based SR methods both in terms of visual and quantitative results. In terms of computational time, the proposed method is somewhat expensive due to the iterative process in the regularization techniques. Multicore parallel processing or general purpose graphics processing units (GP-GPUs) may be an alternative choice for the efficient implementation of this method to achieve clinically feasible performance.

In **Chapter 4**, we present a novel SISR method using sparse reconstruction based on image sparsity and non-local self similarity. Extraction of prior information both external and internal is proved to be very efficient in preserving detailed information in super-resolved clinical DW and MRS images. Visual and quantitative comparisons with state-of-the-art SR methods have demonstrated the superiority of the proposed method. It is validated both for real MR and synthetic images; found its potential to preserve fine details and structures at different upscaling ratios. Finally, use of GP-GPU hardware to get computationally efficient results, makes the proposed algorithm not only highly effective but also practically doable.

Scope for the Future Work

The future work would combine neural networks with nonlocal and statistical priors to preserve the consistency of high-resolution textured patterns, which are missed in the observed low-resolution images.Thus, this may lead to lack of texture information inside images. Moreover, an end-to-to-end network would be proposed for joint super-resolution and segmentation or even joint super-resolution, segmentation and synthesis.

Bibliography

[1] Aharon, M., Elad, M., and Bruckstein, A. M. K-SVD: An algorithm for designing overcomplete dictionaries for sparse representation. *IEEE Transactions on Signal Processing*, 54(11):4311–4322, 2006.

[2] Altay, C., . B. P. The efficiency of diffusion weighted MRI and MR spectroscopy on breast MR imaging. *The Journal of Breast Health*, 10(4):197–200, 2014.

[3] Baker, S. and Kanade, T. Limits on super-resolution and how to break them. *IEEE Transactions on Pattern Analysis and Machine Intelligence*, 24(9):1167–1183, 2002.

[4] Bruce, A. G., Sardy, S., and Tseng, P. Block coordinate relaxation methods for nonparamatric signal denoising. In *SPIE Proceedings*, volume 3391, pages 1–12, 1998.

[5] Candes, E., Braun, N., and Wakin, M. Sparse signal and image recovery from compressive samples. In *4th IEEE International Symposium on Biomedical Imaging: From Nano to Macro*, pages 976–979, 2007.

[6] Candes, E. J., Romberg, J. K., and Tao, T. Stable signal recovery from incomplete and inaccurate measurements. *Communications on Pure and Applied Mathematics: A Journal Issued by the Courant Institute of Mathematical Sciences*, 59(8):1207–1223, 2006.

[7] Ceccarelli, M., di Bisceglie, M., Galdi, C., Giangregorio, G., and Ullo, S. L. Image registration using non-linear diffusion. In *IEEE International Geoscience and Remote Sensing Symposium (IGARSS) 2008*, volume 5, pages 220–223, 2008.

[8] Ceccarelli, M., di Bisceglie, M., Galdi, C., Giangregorio, G., and Ullo, S. L. Image registration using non-linear diffusion. In *IEEE International Geoscience and Remote Sensing Symposium (IGARSS) 2008*, 2008.

[9] Ceccarelli, M., di Bisceglie, M., Galdi, C., Giangregorio, G., and Ullo, S. L. Image registration using non-linear diffusion. In *IEEE International Geoscience and Remote Sensing SymposiumI GARSS 2008*, volume 5, pages 220– 223, 2008.

[10] Chang, K., Ding, P. L. K., and Li, B. Single image super resolution using joint regularization. *IEEE Signal Processing Letters*, 25(4):596–600, 2018.

[11] Chang, K., Ding, P. L. K., and Li, B. Single image super-resolution using collaborative representation and non-local self-similarity. *Signal Processing*, 149:49–61, 2018.

[12] Deka, B. and Datta, S. *Compressed Sensing Magnetic Resonance Image Reconstruction Algorithms: A Convex Optimization Approach*. Springer Series on Bio- and Neurosystems. Springer, Singapore, 2019.

[13] Deka, B., Mullah, H. U., Datta, S., Lakshmi, V., and Ganesan, R. Sparse representation based super-resolution of MRI images with non-local total variation regularization. In 8^{th} *International Conference on Pattern Recognition and Machine Intelligence*. Springer, December 2019.

[14] Dong, C., Loy, C. C., He, K., and Tang, X. Learning a deep convolutional network for image super-resolution. In Fleet, D., Pajdla, T., Schiele, B., and Tuytelaars, T., editors, *Computer Vision 2014, Lecture Notes in Computer Science, Springer*, volume 8692, pages 184–199, 2014.

[15] Dong, W., Shi, G., Li, X., Ma, Y., and Huang, F. Compressive sensing via nonlocal low-rank regularization. *IEEE Transactions on Image Processing*, 23 (8):3618–3632, 2014.

[16] Elad, M., Starck, J.-L., Querre, P., and Donoho, D. Simultaneous cartoon and texture image inpainting using morphological component analysis (MCA). *Applied and Computational Harmonic Analysis*, 19:340–358, 2005.

[17] Fernandez-Beltran, R., Latorre-Carmona, P., and Pla, F. Single-frame super-resolution in remote sensing: a practical overview. *International Journal of Remote Sensing*, 38(1):314–354, 2017.

[18] Fiat, D. Method of enhancing an MRI signal, U.S. patent US6294914B1, filed Sept. 3, 1997, issued Sept. 25, 2001.

[19] Freeman, W. T., Jones, T. R., and Pasztor, E. C. Example-based super-resolution. *IEEE Computer Graphics and Applications*, 22(2):56–65, 2002.

[20] Hardiea, R. C., Barnardb, K. J., Bognarc, J. G., Armstrongc, E. E., and Watsonb, E. A. High-resolution image reconstruction from a sequence of rotated and translated frames and its application to an infrared imaging system. *Optical Engineering*, 37(1):247–260, 1998.

[21] Irani, M. and Peleg, S. Improving resolution by image registration. *CVGIP: Graphical Models and Image Processing*, 53(3):231–239, 1991.

[22] Jain, S., Sima, D. M., Nezhad, F. S., Williams, S., Huffel, S. V., Maes, F., and Smeets, D. Patch based super-resolution of MR spectroscopic images. In *2016 IEEE 13th International Symposium on Biomedical Imaging (ISBI)*, 2016.

[23] Jain, S., Sima, D. M., Nezhad, F. S., Hangel, G., Bogner, W., Williams, S., Van, S. H., Maes, F., and Smeets, D. Patch-based super-resolution of MR spectroscopic images: applicationto multiple sclerosis. *Frontiers in neuroscience*, 11: 1–12, 2017.

[24] Kim, J., Lee, J. K., and Lee, K. M. Accurate image super-resolution using very deep convolutional networks. In *IEEE Conference on Computer Vision and Pattern Recognition (CVPR) 2016*, pages 1646–1654, 2016.

[25] Lee, H., Battle, A., Raina, R., and Ng, A. Y. Efficient sparse coding algorithms. In Schölkopf, B., Platt, J. C., and Hoffman, T., editors, *Proceedings of the 19th International Conference on Neural Information Processing Systems (NIPS)*, pages 801–808, Vancouver, BC, Canada, 2007. MIT Press.

[26] Lu, X., Yuan, H., Yan, P., Yuan, Y., and Li, X. Geometry constrained sparse coding for single image super-resolution. In *IEEE Conference on Computer Vision and Pattern Recognition*, pages 1648–1655, 2012.

[27] Marquina, A. and Osher, S. J. Image super-resolution by tv-regularization and bregman iteration. *Journal of Scientific Computing*, 37(3):367–382, 2008.

[28] Park, S. C., Park, M. K., and Kang, M. G. Super-resolution image reconstruction: a technical overview. *IEEE Signal Processing Magazine*, 20(3):21–36, 2003.

[29] Peleg, T. and Elad, M. A statistical prediction model based on sparse representations for single image super-resolution. *IEEE Transactions on Image Processing*, 23(6):2569–2582, 2014.

[30] Plenge, E., Poot, D. H. J., Bernsen, M., Houston, G. K. G., Wielopolski, P., van der Weerdand Wiro J. Niessen, L., and Meijering, E. Super-resolution methods in MRI: Can they improve the trade-off between resolution, signal-to-noise ratio, and acquisition time? *Magnetic resonance in medicine*, 68(6): 1983–1993, 2012.

[31] Reeth, E. V., Tham, I. W. K., Tan, C. H., and LooPoh, C. Super-resolution in magnetic resonance imaging: A review. *Concepts in Magnetic Resonance*, 40 (6):306–325, 2012.

[32] Ren, C., He, X., Teng, Q., Wu, Y., and Nguyen, T. Q. Single image super-resolution using local geometric duality and non-localsimilarity. *IEEE Transactions on Image Processing*, 25(5):2168–2183, 2016.

[33] Rueda, A., Malpica, N., and Romero, E. Single-image super-resolution of brain MR images using overcomplete dictionaries. *Medical Image Analysis*, 17(1): 113–132, 2013.

[34] Shi, F., Cheng, J., Wang, L., Yap, P.-T., and Shen, D. LRTV: MR image super-resolution with low-rank and total variation regularizations. *IEEE Transactions on Medical Imaging*, 34(12):2459–2466, 2015.

[35] Shi, F., Cheng, J., Wang, L., Yap, P.-T., and Shen, D. LRTV: MR image super-resolution with low-rank and total variation regularizations. *IEEE Transactions on Medical Imaging*, 34(12):2459–2466, 2015.

[36] Sun, J., Xu, Z., and Shum, H.-Y. Image super-resolution using gradient profile prior. In *IEEE Conference on Computer Vision and Pattern Recognition*, pages 1–8, 2008.

[37] Tsai, R. Y. and Huang, T. S. Multiframe image restoration and registration. *Advances in Computer Vision and Image Processing*, 1:317–339, 1984.

[38] Wang, Q. and Ward, R. K. A new orientation-adaptive interpolation method. *IEEE Transactions on Image Processing*, 16(4):889–900, 2007.

[39] Xie, J., Feris, R. S., and Sun, M.-T. Edge-guided single depth image super resolution. *IEEE Transactions on Image Processing*, 25(1):428–438, 2015.

[40] Xu, J., Zhang, L., Zuo, W., Zhang, D., and Feng, X. Patch group based non-local self-similarity prior learning for image denoising. In *IEEE International Conference on Computer Vision (ICCV)*, pages 244–252, 2015.

[41] Xue, W., Zhang, L., Mou, X., and Bovik, A. C. Gradient magnitude similarity deviation: A highly efficient perceptual image quality index. *IEEE Transactions on Image Processing*, 23:684–695, 2013.

[42] Yang, J., Wang, Z., Lin, Z., Cohen, S., and Huang, T. Coupled dictionary training for image super-resolution. *IEEE Transactions on Image Processing*, 21:3467–3478, 2010.

[43] Yang, J., Wright, J., Huang, T. S., and Ma, Y. Image super-resolution via sparse representation. *IEEE Transactions on Image Processing*, 19(11):2861–2873, 2010.

[44] Yang, M.-C. and Wang, Y.-C. F. A self-learning approach to single image super-resolution. *IEEE Transactions on multimedia*, 15(3):498–508, 2012.

[45] Yu, S., Zhang, R., Wu, S., Hu, J., and Xie, Y. An edge-directed interpolation method for fetal spine MR images. *BioMedical Engineering OnLine*, 12(102): 1–12, 2013.

[46] Zha, Z., Zhang, X., Wang, Q., Bai, Y., Chen, Y., Tang, L., and Liu, X. Group sparsity residual constraint for image denoising with external non-local self-similarity prior. *Neurocomputing*, 275:2294–2306, 2018.

[47] Zhang, D., He, J., and Zhao, Y. Brain MR image super-resolution reconstruction via sparse representationand non-local similarity regularisation. *International Journal of Biomedical Engineering and Technology*, 15(2):95–113, 2014.

[48] Zhang, D., He, J., Zhao, Y., and Du, M. MR image super-resolution reconstruction using sparse representation,nonlocal similarity and sparse derivative prior. *Computers in Biology and Medicine*, 58:130–145, 2015.

[49] Zhang, J., Liu, S., Xiong, R., Ma, S., and Zhao, D. Improved total variation based image compressive sensing recovery by nonlocal regularization. In *IEEE International Symposium on Circuits and Systems (ISCAS) 2013, Beijing, China*, pages 2836–2839, 2013.

[50] Zhang, K., Gao, X., Tao, D., and Li, X. Single image super-resolution with non-local means and steering kernelregression. *IEEE Transactions on Image Processing*, 21(11):4544–4556, 2012.

[51] Zhang, L., Zhang, L., Mou, X., and Zhang, D. FSIM: A feature similarity index for image quality assessment. *IEEE Transactions on Image Processing*, 20(8): 2378–2386, 2011.

[52] Zhang, L., Zhang, L., Mou, X., and Zhang, D. FSIM: A feature similarity index for image quality assessment. *IEEE transactions on Image Processing*, 20(8): 2378–2386, 2011.

[53] Zhang, X., Lam, E. Y., Wu, E. X., and Wong, K. K. Application of Tikhonov regularization to super-resolution reconstruction of brain MRI images. In *International Conference on Medical Imaging and Informatics*, pages 51–56. Springer, 2007.

[54] Zontak, M., Mosseri, I., and Irani, M. Separating signal from noise using patch recurrence across scales. pages 1195–1202, 2013.

List of Publications

(i) Bhabesh Deka, Sumit Datta, Helal Uddin Mullah and Suman Hazarika, "Diffusion-weighted and Spectroscopic MRI Super-resolution using Sparse Representations", *Biomedical Signal Processing and Control*, vol. 60, 2020.

(ii) Bhabesh Deka, Helal Uddin Mullah, Sumit Datta, V Lakshmi, R Ganesan, "Sparse representation based super-resolution of MRI images with non-local total variation regularization", *SN Computer Science, Springer*, vol. 1, pp. 1-13, 2020.

(iii) Bhabesh Deka, Helal Uddin Mullah, Sumit Datta, V Lakshmi, R Ganesan, "Sparse Representation Based Super-Resolution of MRI Images with Non-Local Total Variation Regularization", *Pattern Recognition and Machine Intelligence, LNCS, Springer*, vol. 11942, pp. 78-86, 2019.